

Partnership for the Assessment of Risks from Chemicals

Deliverable 5.2: 1st New PBK Models Report

WP5 – Task 5.3



| Technical reference | |
|----------------------------------|-------------------------------------------------------------------------------------------------------------------------------------------------------------------------------------------------------------------------------------------------------------------------------|
| Work package | WP5 – Hazard Assessment |
| Task | Task 5.3 - Quantitative systems toxicology and development of new AOPs |
| Dissemination level ¹ | Public |
| Lead Beneficiary/ Responsible AE | ITEM ETHZ |
| Responsible author(s) | Project leaders: Sylvia Escher, ITEM and Georg Aichinger, ETHZ Case study teams: CS1: ETHZ , WR, IISPV, UNIVIE CS2: IISPV , WR CS3: ISS , ITEM, INERIS CS4: INERIS , ITEM, AUTH CS5: IISPV , BfR |
| Co-authors | Wageningen Food Safety Research, Wageningen University and Research, Akkermaalsbos 2, 6708 WB, Wageningen, the Netherlands |
| Internal Reviewers ² | Philip Marx-Stoelting/BfR/ Philip.Marx-Stoelting@bfr.bund.de Gilles Rivière/Anses/ gilles.riviere@anses.fr |
| External Reviewers ³ | Pascal Sanders/Anses/pascal.sanders@anses.fr Emma Di <u>Consiglio/ISS/emma.diconsiglio@iss.it</u> Jean-Lou Dorne /Jean-Lou.DORNE@efsa.europa.eu |
| Due date of deliverable | April 2025 |
| Actual submission date | 25/06/2025 |

¹ PU = Public

Document history

| Version | Date | Reviewer name/Institutions | Short description of changes |
|---------|------------|---------------------------------|------------------------------------------------------|
| 1 | 31/03/2025 | Sylvia Escher/Georg Aichinger | 1 st version of the deliverable submitted |
| 2 | April 2025 | External reviewers | 1 th Review of the deliverable |
| 3 | June 2025 | Main authors and WP5 co-leaders | Comments of reviewers addressed |

“Funded by the European Union. Views and opinions expressed are, however, those of the author(s) only and do not necessarily reflect those of the European Union or the Health and Digital Executive Agency. Neither the European Union nor the granting authority can be held responsible for them.”

Abstract

PARC develops next generation risk assessment (NGRA) approaches to assess the toxicity of compounds for which *in vivo* animal data is lacking. NGRA mainly relies on new approach methods (NAMs), which include *in silico* and human centric *in vitro* models. One central aspect in NGRA is the derivation of relevant human thresholds, that are derived from *in vitro* benchmark concentrations via quantitative *in vitro* to *in vivo* extrapolation (QIVIVE). QIVIVE relies on two aspects, on a reliable estimate of the *effective in vitro* reference concentrations and on physiologically based kinetic modelling approaches, which are used to estimate the corresponding plasma and tissue concentration as well as human equivalent dose.

D5.3 addresses the latter and has developed a series of case studies in order to evaluate NAM based approaches to model the absorption, distribution, metabolism and excretion of chemicals and consequently their bioavailable fraction in the human organism. This deliverable reports the recent results of the following five case studies (CSs):

1. **CS-1: The impact of the human microbiome on xenobiotic metabolism**
2. **CS-2: ADME properties of PFAS**
3. **CS-3: Integration of Isoform Specific Metabolism into PBK models**
4. **CS-4: Develop a tiered testing for inhalable compounds**
5. **CS-5: The role of the blood brain barrier in PBK models**

Several other case studies are ongoing, e.g. Alternaria toxins (UNIVIE), enniatins (ANSES) and metabolic disruption (UDE), while three more case studies on the placental barrier (WUR), phthalates (Unisante) and assessment of airborne compounds (RIVM) will start in the fourth year of the PARC project. The case studies aim at a better understanding of PBK models for xenobiotics and the remaining uncertainties. Such case studies are useful to illustrate these aspects and to gain more experience and confidence in these approaches. In parallel, data and knowledge gaps will be filled. The improved testing and modelling approaches will be integrated into NGRA approaches in the future, e.g. in the context of WP6 case studies or regulatory risk assessment approaches.

Key Words

Method development, physiologically-based kinetic modelling, New Approach Methods, *in vitro* to *in vivo* extrapolation, intrinsic metabolic clearance, gut microbiome, QSAR

Table of contents

| | |
|---------------------------------------------------------------------------------------------------------------------------|----|
| Document history _____ | 3 |
| Abstract _____ | 4 |
| Key Words _____ | 4 |
| Authors and Acknowledgements _____ | 6 |
| Acronyms _____ | 6 |
| 1. Background _____ | 6 |
| 2. Case study 1- Human Microbiome (ETHZ, WR, IISPV, UNIVIE) _____ | 7 |
| 2.1 Case study Background and Objectives _____ | 7 |
| 2.2. Approach _____ | 7 |
| 2.3. Results _____ | 11 |
| 2.4. Discussion _____ | 14 |
| 3. Case study 2- ADME properties of PFAS (IISPV, WR) _____ | 15 |
| 3.1 Case study Background and Objectives _____ | 15 |
| 3.2. Approach _____ | 15 |
| 3.3. Results _____ | 17 |
| 3.4. Discussion _____ | 19 |
| 4. Case study 3 - Integration of Isoform Specific Metabolism into PBK models - example Organophosphates (ISS, ITEM) _____ | 20 |
| 4.1 Case study Background and Objectives _____ | 20 |
| 4.2. Approach _____ | 20 |
| 4.3. Results _____ | 23 |
| 5. Case study 4 - Develop a tiered testing for inhalable compounds (INERIS, ITEM, AUTH) _____ | 25 |
| 5.1 Case study Background and Objectives _____ | 25 |
| 5.2. Approach _____ | 25 |
| 5.3. Results _____ | 28 |
| 5.4 Conclusion _____ | 31 |
| 6. Case study 5 - The role of the blood brain barrier in PBK models (BfR, IISPV) _____ | 32 |
| 6.1 Case study Background and Objectives _____ | 32 |
| 6.2. Approach _____ | 32 |
| 6.3. Results _____ | 34 |
| 6.4. Discussion _____ | 36 |
| 7. Conclusion _____ | 37 |
| 8. References _____ | 38 |

Authors and Acknowledgements

The Task 5.3.4 (co)leaders would like to thank all 5.3.4 partners for their contribution (details in the Annex section).

Acronyms

ADME: Absorption, distribution, metabolism or excretion

CYP: cytochrome P450

EHC: Enterohepatic circulation

IVIVE: In Vitro to In Vivo Extrapolation

NAMs: New Approach Methodologies

NGRA: Next generation risk assessment

PBK: Physiologically based kinetic

PFAS: Per- and PolyfluoroAlkyl Substances

QIVIVE: Quantitative in vitro / in vivo Extrapolation

QSAR: Quantitative structure activity relationship

1. Background

In Vitro to In Vivo Extrapolation (IVIVE) is a central part of Next Generation Hazard and Risk assessment (NGRA). It allows to set human relevant thresholds based on integrated approaches to testing and assessment.

The PARC project actively contributes to the development of generic physiologically based kinetic models, which use New Approach Methods, like in silico and in vitro models, to characterize the compounds specific parameter on absorption, distribution, metabolism or excretion (ADME). The new modeling approaches are worked out in case studies, which address specific data and knowledge gaps.

The main results per case study are in the following sections reported. Each case study reports the objectives of the case study, a rationale for model compound selection, the testing and assessment strategy as well as the modeling results. The final section provides a discussion on main achievements and perspectives with regard to so far identified remaining data and knowledge gaps. The knowledge gaps cannot be filled by PARC in isolation, therefore several other projects like the RISKHUNT3R and the EFSA ADME4NGRA project support this development, conducting complementary case studies.

2. Case study 1- Human Microbiome (ETHZ, WR, IISPV, UNIVIE)

2.1 Case study Background and Objectives

2.1.1 Short Intro - describe the state of the art

Metabolic transformations of xenobiotic chemicals are well-established critical factors in chemical risk assessment. Recently, the gut microbiome has emerged as a key contributor to chemical metabolism. However, our ability to predict microbial metabolism and perturbations is limited and still relies on expensive, slow and ethically questionable *in vivo* studies. Furthermore, most data concerns how the genomic composition of microbial communities are altered by chemical exposures or disease states, whereas key information regarding metabolic functionality and its impact on toxicant disposition is lacking, in particular for natural toxins. Developing *in vitro* test systems and computational models that allow for integrating microbial metabolism into risk assessment is central to chemical safety. To this end, microbiome-competent PBK modeling is a promising tool to quantitatively predict human internal exposures to microbially activated xenobiotics.

2.1.2 List the case study objectives

The overall objective of this case study is to establish harmonized methods to evaluate gut microbial metabolism kinetics and include them in PBK models to accurately predict ADME processes that are impacted by gut microbiota. This includes:

- development of an optimized high-throughput fecal fermentation assay coupled with LC-MS/MS and evaluation of different factors (sample freezing, dilution, interindividual differences) by tracking the degradation of a set of chemical tracer probes representing distinct biotransformation reactions known to be catalyzed by human gut microbiomes.
- development of QSAR tools for quantitatively predicting biliary excretion kinetics of hepatic phase II metabolites as a prerequisite of accurately including enterohepatic circulation (EHC) in PBK modeling. The model focus on transporters that govern the rate of excretion via bile e.g. MRP2/3/4.
- evaluation of existing *in silico* strategies to conceptually include gut microbial biotransformation in PBK modeling and, based on that, the recommendation of harmonized approach for future microbiome-competent PBK modeling.

2.2. Approach

2.2.1 Selection of model compounds

Mass spectrometric metabolomics assays based on chemical tracer probes (Fig. 1) were used to profile the impact of chemical-gut microbiota interactions. Those chemicals were selected based on previously published evidence to undergo gut microbial biotransformation. For biliary excretion QSAR development, a score of chemicals for which data on substrate affinity of transporter proteins was available was extracted from literature. For evaluation of developed methods, three previously published microbiome-competent PBK models are reparameterised for the following gut microbial biotransformation reactions: ellagic acid to urolithin A; daidzein to s-equol; zearalenone to α/β -zearalenol.

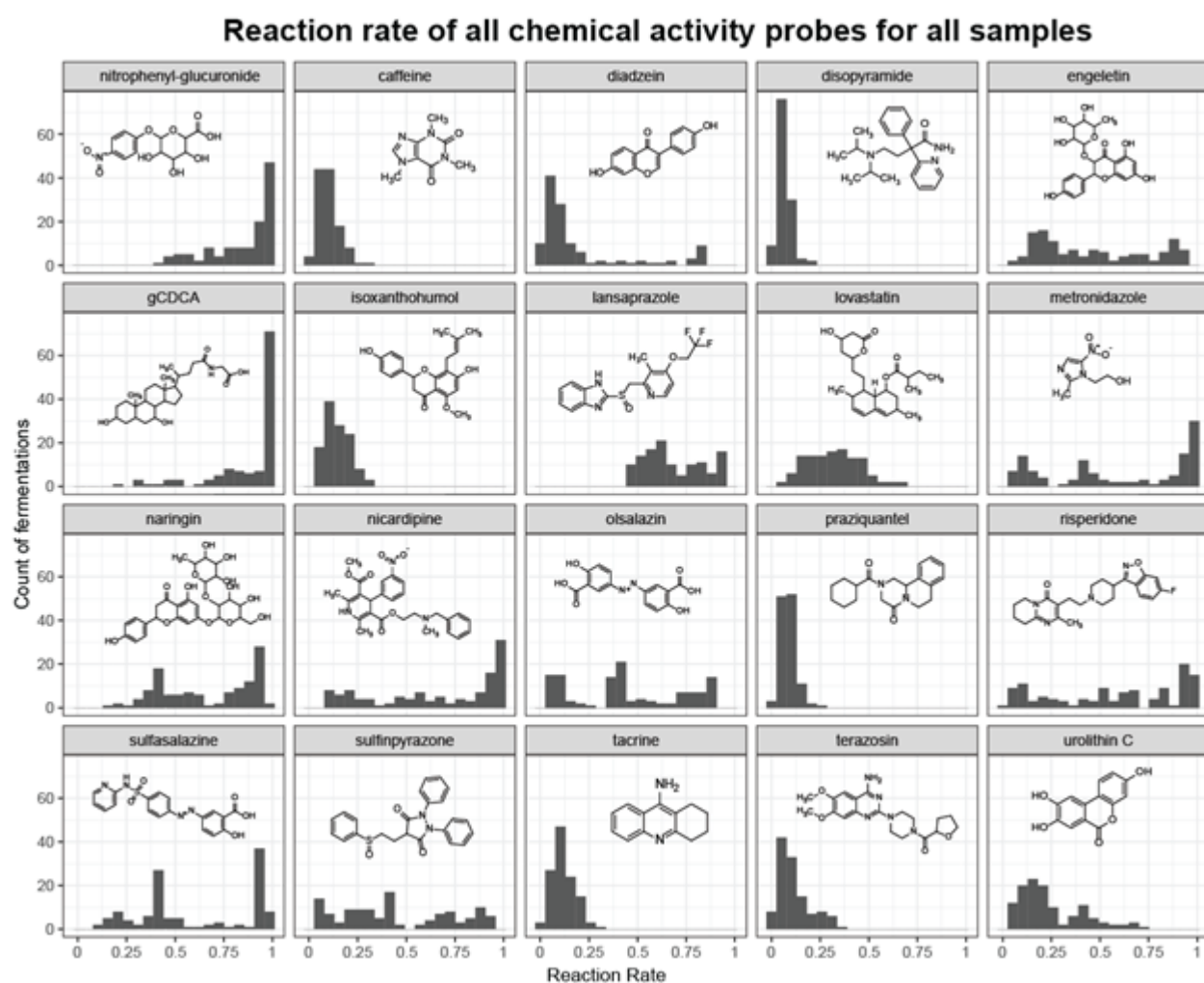


Fig. 1: Chemical probes for fecal fermentation assays and corresponding normalized reaction rates measured in all conducted experiments.

2.2.2 NAM methodologies

For optimising *ex vivo* fecal fermentation methodology for chemical biotransformation testing, we collected stool samples from 5 healthy individuals and prepared fecal slurries in PBS. Fecal fermentations were carried out at 37°C under anaerobic conditions in deep 96-well plates. At the start of each fermentation, the fecal slurry was spiked with a mixture of chemical probes for metabolic profiling. Samples were taken 0, 3, 6, and 24h and the degradation of chemical probes was analyzed by LC-MS/MS. The impact of the following conditions on microbial biotransformation rates were tested: inter-donor variance; fresh fecal slurry vs. fecal slurry that was stored frozen at -80°C for at least 48h; use of PBS vs. complete growth medium (BYCFA + 6C + muc); use of different dilution factors. Chemical degradation rates were calculated from AUC and results were compared by linear regression models. In addition to targeted analysis, LC-MS/MS based untargeted metabolomics were carried out using a ThermoFisher Orbitrap ID-X Tribrid mass spectrometer.

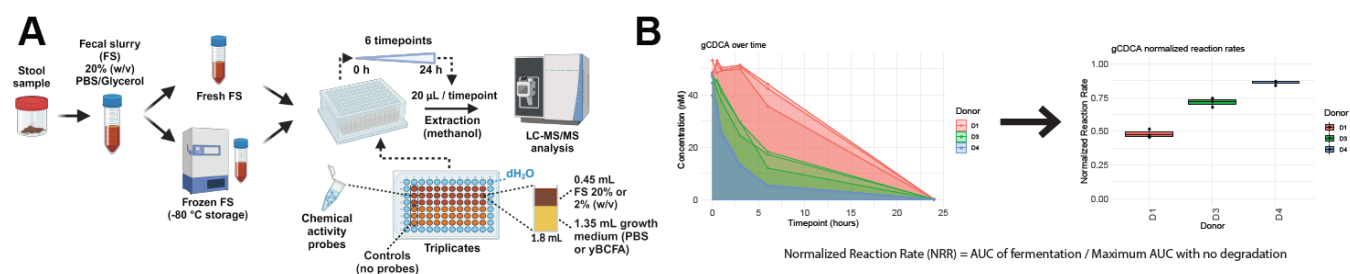


Fig 2. A. Schematic representation of the treatment of stool samples after collection, fermentation assay, and sample analysis. B. Two graphs present the conversion of time series concentration information to normalized reaction rate (NRR) values.

For QSAR development to facilitate inclusion of EHC in PBK modeling, we compiled a dataset containing clearance-related values of glucuronide compounds through hepatic transporters: MRP2, MRP3, MRP4, and BCRP. These values were standardised and adjusted to account for discrepancies resulting from diverse experimental conditions using QIVIVE (Quantitative In Vitro to In Vivo Extrapolation) approaches. Next, we developed a Quantitative Structure-Activity Relationship (QSAR) model to predict clearance values for glucuronidated compounds in each of these transporters. The model was constructed based on relevant molecular descriptors and physicochemical properties of the training dataset and validated to ensure its robustness and predictive accuracy. Finally, we integrated the predicted clearance values into the parameterisation of human PK models. Subsequently, we compared the newly generated PK model predictions of *in vivo* systemic concentrations with no-EHR refined models and validation data to assess our method's capacity to enhance the predictive capabilities of PK modeling.

NAM methodology to parameterize microbiota-based PBK model

IISPV conducted some *in vitro* studies at ETHZ to evaluate how BPA, TDCPP and PFOA affect the metabolism of the gut microbiota isolated from fecal samples from different healthy donors, with the intention to use respective results in developing microbiome-competent PBK models for these chemicals. The idea was to obtain time-dependent metabolic patterns for three chemicals that can be used to calculate microbiota-based clearance parameters using IVIVE strategy. Later, the conditioned media was used further for in-vitro immunotoxicity studies. However, the results obtained related to immunotoxicity were not conclusive, so the experiments are still ongoing.

Different concentrations of the compounds were tested based on literature data, using as a reference the daily intake in humans defined by the EFSA. Fresh fecal samples were collected from five healthy adult donors (1 female and 4 males), and in an anonymized, non-interventional manner. All samples were processed within 3 hours of collection inside an anaerobic chamber. To prepare a 20% (w/v) fecal slurry (FS), 8g of fecal matter homogenized with 40 mL of anaerobic phosphate buffer (PBS) containing glycerol 15% (v/v) using glass beads and a vortex. The mixture was filtered and stored at -80°C. A pooled FS sample was prepared by combining 10 mL of each individual FS.

Fecal microbiota was cultivated in bYCFa medium supplemented with heat-stable 6C+Muc components. Fermentation assays were performed in 96-deepwell plates (1.8 mL). Individual and pooled FS 20% (w/v) were diluted with complete medium to achieve a final FS concentration of 5% (w/v). The medium was supplemented with BPA, TDCPP or PFOA at a final concentration of 7.5, 37.5 or 75 µM. Outer wells were filled with dH₂O or PBS to reduce evaporation. Samples (20 µL) were collected at 0, 4 and 24h, and transferred to a 96-well plate containing 180 µL of methanol 100% (v/v) and sulfamethoxazole as internal standard for mass spectrometry. The 96-well plates were quickly sealed and stored at -20°C.

2.2.3 Analytical methods

Chemical analysis was performed using targeted and untargeted LC-MS/MS approaches with a Tribrid IDX (ThermoFischer) mass spectrometer and LC techniques including reversed phase (RP) and hydrophilic interaction liquid chromatography (HILIC). Tandem MS was used to quantify chemical targets while data dependent MS/MS acquisition is used for untargeted metabolite identification. Targeted data was processed through open-source software Skyline, while untargeted data was processed through open-source software MSDIAL (github: <https://github.com/systemsomicslab/MsdialWorkbench>).

Chemicals were measured using a Vanquish HPLC (ThermoFisher) linked with an IDX tribrid LC-MS/MS mass spectrometer (ThermoFisher) for TDCPP, BPA, and PFOA. Resuspended samples were stored in the autosampler at 4 °C until analysis. Injection volume was 5 µL. A Synergi 30 mm x 2 mm (4 µm Polar-RP 80 Å) LC column (Phenomenex) was kept at 40 °C and had a constant flow rate of 0.7 mL per minute. Mobile phase A was LC-MS grade water with 0.1% formic acid, and mobile phase B was LC-MS grade acetonitrile with 0.1% formic acid. The LC gradient was 5% B from 0 to 0.1 minutes, brought to 100% B between 0.1 and 1.8 minutes, kept at 100% B until 2.35 minutes, brought to 5% B between 2.35 and 2.4 minutes, and kept at 5% B from 2.4 to 2.8 minutes. The autosampler needle wash and injection process took approximately 1 minute between each sample. Ionization source conditions for sheath gas, aux gas, and sweep gas were 60, 15, and 2 respectively. The transfer tube was at 350 °C, and the vaporizer temperature was 400 °C. MS1 spectra were acquired at 60k resolution between 60-800 m/z with RF lens of 45%, and maximum injection time of 50 ms with default AGC target. Targeted MS/MS scans were performed using the linear ion trap with fragmentation energy and RF lens% values optimized to each targeted metabolite. Both positive and negative ionization modes were employed on separate injections with +3.5 kV and -2.5 kV spray voltages. For identification of non-targeted LC-MS features, a pooled sample was analyzed 9 times with iterative exclusion data dependent MS/MS spectra acquired at 15k resolving power in the orbital ion trap and the top two ions selected for fragmentation using 2.5 second dynamic exclusion.

Untargeted MS/MS analysis in positive and negative ionization mode was used to quantify the concentrations of chemicals during fermentation with both individual and pooled FS samples. Raw data were first corrected using an internal standard, and the resulting values were interpolated against a standard calibration curve to determine the final concentrations of each compound at 0, 4 and 24 hours of fermentation. An untargeted metabolomic approach was performed using MS/MS in positive ionization mode, which resulted in the detection of approximately 6,816 distinct metabolites. For this analysis, only pooled (FS) were used. Cells were exposed to BPA, TDCPP, PFOA at concentrations of 7.5 µM. Samples were collected at 0, 4, and 24h post-exposure. For statistical analysis, the intensity values recorded by the mass spectrometer for each experimental condition were compared to the DMSO-treated control using a student's t-test. In addition, fold changes were calculated and used in combination with the p-values to construct volcano plots, plotting the $-\log_{10}(\text{p-value})$ against the $\log_2(\text{fold change})$.

2.2.4 PBK modelling

Accurate parameterisation of the gastrointestinal tract is important for microbiome-competent PBK modeling. Apart from volumes of stomach, small and large intestine which have been previously estimated and widely used in PBK modeling, this includes parameters for gastrointestinal passage times (Wang et al., 2015) as well as gastrointestinal absorption. The latter is taken from experimentation using the Caco-2 monolayer model with subsequent use of the algorithm of Sun et al. (2002) for scaling. The impact of differing gastrointestinal compartment conceptualization and different factors for in vitro to in vivo scaling of microbial biotransformation on predicted blood levels of gastrointestinal metabolizes is tested for three parent – metabolite couples with published PBK models. We compare the performance of standard models with the split colon method of Mendez-Catala et al. (2021). Further, we compare scaling by wet and dry fecal weight as well as bacterial count. All these modifications are evaluated for accuracy of predictions against a) the originally published models and b) available human pharmaco- / toxicokinetic data.

2.3. Results

2.3.1 Optimization of fecal fermentation assays for gut microbial biotransformation testing

We compared targeted analysis data of chemical degradation in fecal fermentation by mixed linear modeling to evaluate the impact of donor individuality, slurry dilution, freezing and modulating effects of the addition of chemical probes across all incubations (Fig 3). As expected, dilution of the fecal slurry lead to a decrease in degradation rates for most chemical probes, with the exception of lovastatin. The choice of suspension solvent (PBS or BYCFA medium) significantly impacted several biotransformation reactions. Contrary to our expectations, freezing the fecal slurry for storage did not impact gut microbial xenobiotic metabolism.

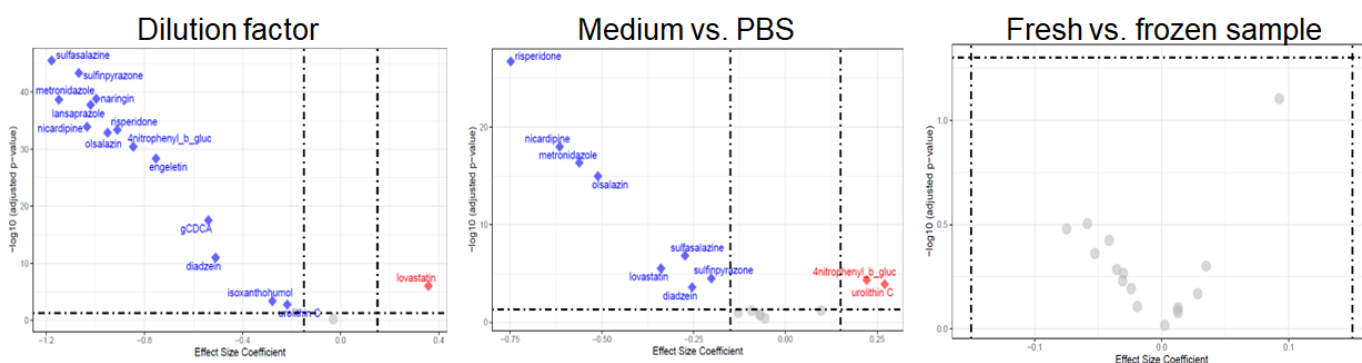


Fig. 3: Effect of fermentation treatment conditions on reaction rate for chemical activity probes. A. Effect of fecal slurry dilution level on reaction rate (5% fecal slurry for concentrated inoculum and 0.5% for dilute inoculum). B. Effect of fresh compared to frozen fecal slurry used in batch fermentations. C. Effect of growth medium (nutrient media yBCFA or PBS). Linear mixed effect models calculated *p*-values and effect size coefficient. Benjamini-Hochberg method was used to correct *p*-values for multiple comparisons.

Further, degradation rates separated by donor in PCA plots, thus demonstrating how interindividual differences in microbial composition impact chemical biotransformation capacities (Fig. 4).

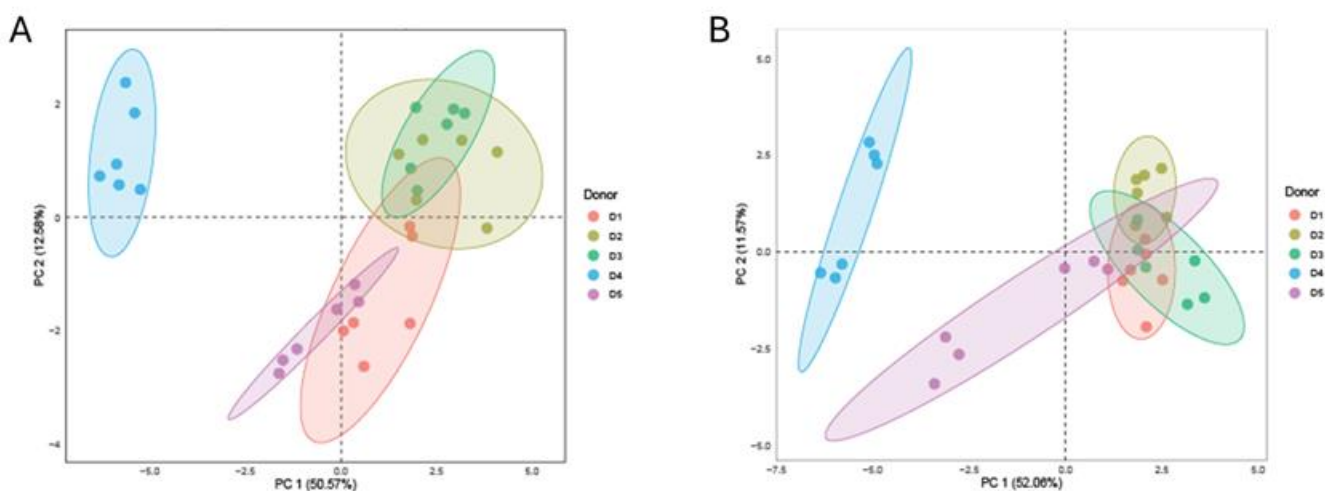


Fig. 4: PCA score plot of reaction rates by donor in A) PBS and B) BYCFA + 6C + Muc

2.3.2 QSAR development for biliary excretion of glucuronides and sulfates

Both a random forest as well as a linear regression model returned sufficient correlation of MRP2-dependent biliary clearance with reported values for the test set (Fig. 5A). Further, we demonstrated that including the QSAR-predicted biliary excretion in previously established PBK models for bisphenol S and urolithin A with assumed quantitative microbial glucuronide cleavage in the small intestine improved their accuracy in predicting blood concentrations (Fig. 5B).

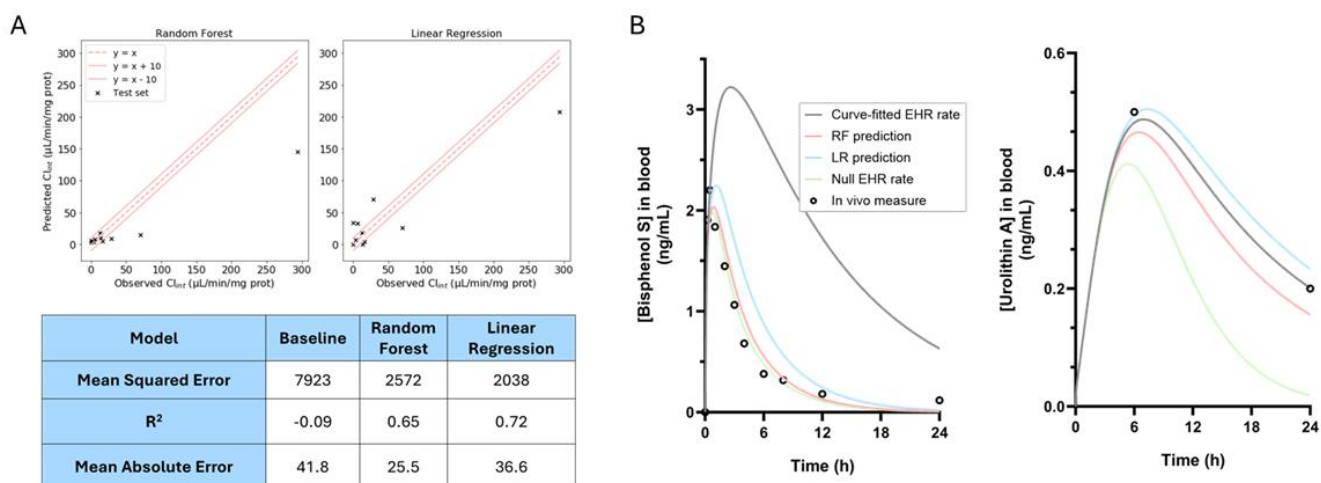


Fig. 5: A QSAR to predict biliary excretion of glucuronides via MRP2. A) Random Forest and Linear Regression model performance compared to test set values (black dots). B) EHC-corrected PBK model predictions compared to original model predictions and in vivo measures. RF: Random Forest, LR: Linear Regression.

2.3.3 Gut microbial metabolism of BPA, TDCCP and PFOA

Figure 2.3.3 represents the metabolisms of TDCPP and PFOA after exposure to fecal samples. No metabolism could be observed at any concentration for PFOA when pooled or individual fecal samples were used. Instead, the measured concentration is higher than the initial one (Fig. 2.3.3.). For TDCPP, 4 out of 5 individual fecal samples resulted in decreased concentrations of the chemicals after 24h. However, this effect was attenuated or not present when pooled samples were used. Metabolomic results (Fig. 2.3.4.) show how the metabolic profile of the microbiota changed after chemical exposure. It was observed that the compounds resulted in significant variation of the metabolic profile in a compound-dependent and concentration-dependent manner, with greater differences at higher concentrations (lower concentrations not shown) which can be used in future for parameterizing the microbiota-based PBK models. Overall, the results show that the susceptibility of environmental contaminants to be metabolized depends on microbiota composition, and that the effect of chemical exposure on the metabolism of the gut microbiota is compound specific.

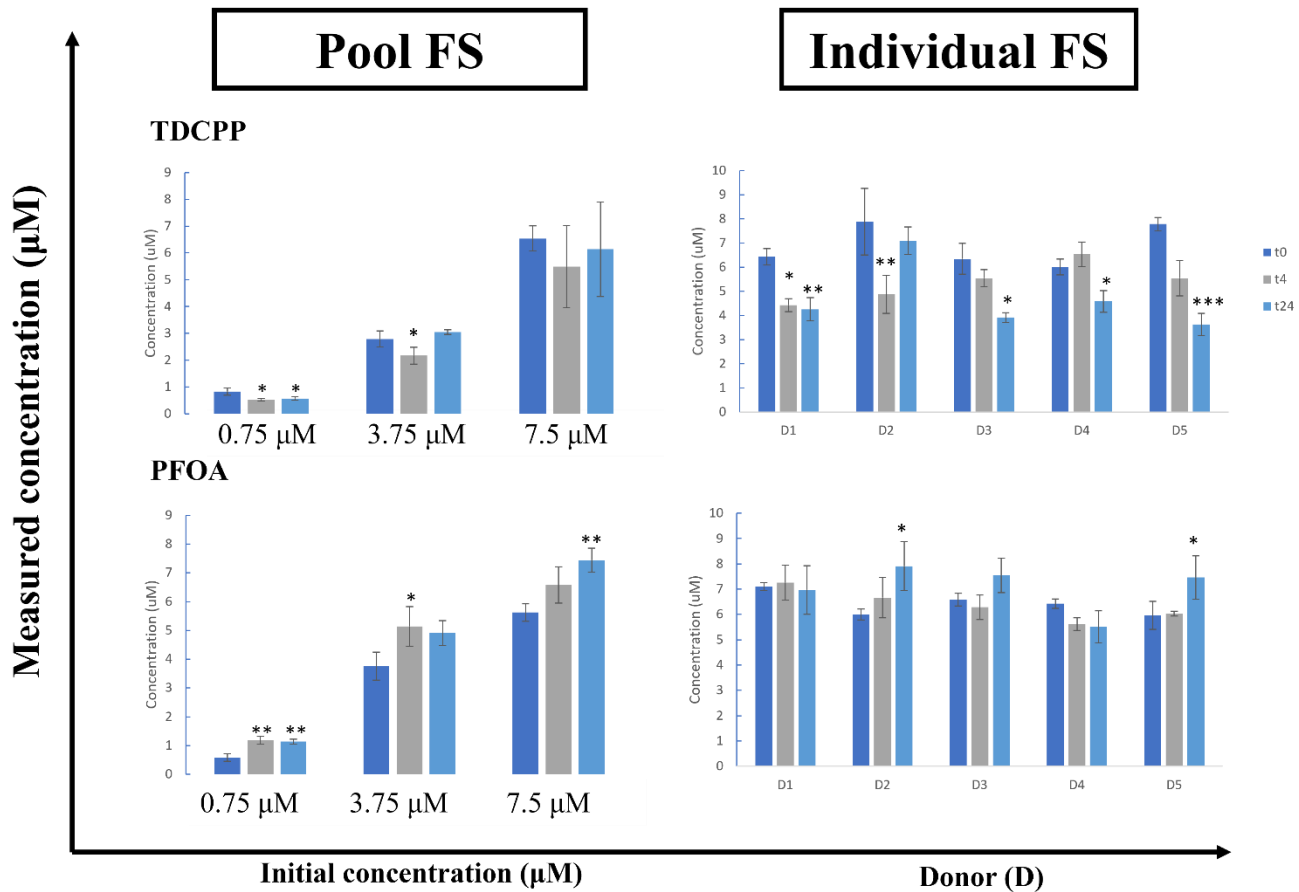


Figure 2.3.3.:

Targeted detection of TDCPP and PFOA in pooled or individual fecal slurry (FS) by LC-MS/MS. Three different initial concentrations (0.75, 3.75, and 7.5 µM) of each chemical were employed. The pooled FS was fermented in the presence of all three concentrations for 0, 4, and 24 hours, whereas individual donors were exposed only to the highest concentration of each chemical. Data represents the mean ± standard deviation (SD) of three independent replicates (n=3). Statistical significance was determined using Dunnett’s multiple comparison test: *p < 0.05, **p < 0.01 and ***p < 0.001.

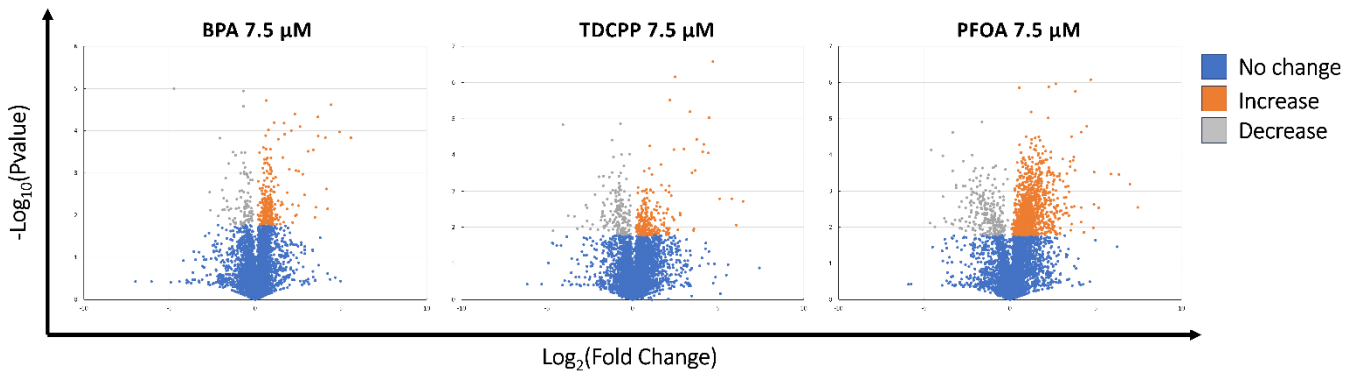


Figure 2.3.4.: Volcano plots from the untargeted metabolomic analysis of pooled fecal slurry (FS) using LC-MS/MS. Fermentation was carried out for 24 hours in the presence of BPA, TDCPP, and PFOA (7.5 µM; n = 3). A total of 6,816 distinct metabolites were detected. Student’s t-test was used to compare metabolite concentrations between

DMSO-treated controls and chemical-exposed samples. Fold changes and p-values were used to generate the plots, with $-\log_{10}(p\text{-value})$ plotted against $\log_2(\text{fold change})$. Blue dots indicate unchanged metabolites, orange represent increased concentrations in chemically treated samples, and grey indicates decreased concentrations.

2.4. Discussion

We optimised a high-throughput fecal fermentation assay for assessing gut microbial chemical biotransformation. Results underscore the importance of considering interindividual differences by testing individual slurries in addition to pooled microbiomes. Also, we can recommend to test and account for microbiome dilution and the impact of suspension solvents before assessing biotransformation kinetics for microbiome-competent PBK modeling. A key result is the insensitivity of bacterial metabolic enzymes to freezing, which will allow researchers to abstain from working with fresh fecal samples and store microbiomes for biotransformation testing, thus reducing practical limitations and increasing possibilities in experimentation, including the reproduction of experiments. The evaluation of the impact of using the optimized protocol on microbiome-competent PBK model accuracy, the evaluation of inter-donor variability as well as an evaluation of *in vitro* to *in vivo* scaling factors are still ongoing.

We developed a first of a kind QSAR tool for quantitatively predicting biliary excretion. Even in its preliminary form (i.e., only considering MRP2, but neglecting the contribution of MRP3, MRP4 and BCRP), it was demonstrated to improve PBK model accuracy of two exemplary compounds that undergo glucuronidation and subsequent EHC. A QSAR tool that includes further transporter proteins and considers sulfates is still under development.

A major limitation of microbiome-competent PBK modeling is the dependency on fecal microbiome samples. The current methodology cannot account for differences in xenobiotic metabolism across sections of the gastrointestinal tract, thus increasing uncertainty. Further, due to the complexity of gut microbial composition, the development of a “one fits all” method for biotransformation testing seems unlikely to be achieved in the near future. We did, however, advance our means of respective testing, and were able to give clear recommendations on preliminary experiments to confirm the applicability of our optimized fecal fermentation protocol prior to its use. In an upcoming project for PARC years 5-7, we will compare this method with methods developed in the EFSA ADME4NGRA project.

3. Case study 2- ADME properties of PFAS (IISPV, WR)

3.1 Case study Background and Objectives

Perfluorinated compounds (PFAS) are considered long-acting chemicals accumulating in humans, animals and the environment with the potential to affect human (and animal) health. Over the past 15 years, various PBK models were developed for four PFASs by different researchers. Among these, the model proposed by Loccisano et al. (2011) has gained widespread acceptance. This model, originally designed for monkeys, was later extrapolated for human use (Loccisano et al., 2011). In 2012, Loccisano (Loccisano et al., 2012) further developed a model for adult rats targeting similar compounds; however, notable structural differences between the rat and human models were observed (Loccisano et al., 2012). These discrepancies pose challenges in extrapolating rat models to humans, especially when human data is limited. For compounds like perfluorononanoic acid (PFNA) and perfluorohexanesulfonic acid (PFHxS) which also accumulate and show to be persistent in humans with long half-lives, currently there are limited PBK models. Notably, Kim et al. (2019). developed a rat model for PFNA with a different structure, yet incorporating nearly identical compartments as Loccisano, albeit with some variations (Kim et al., 2019). Recognizing these limitations in existing models and the varied structures for PFAS compounds within the same chemical group, we have undertaken the initiative to construct a generic model applicable to both rats and humans. This model is based on the structural framework proposed by Deepika et al. (2021)¹.

The aim of this case study is to evaluate whether a chemical-specific human PBK model (PFOA and PFOS) can be extended to include description of kinetics of related chemicals (PFNA, PFHxS) in humans based on 'scaling' of chemical-specific parameter values (uptake rate, plasma protein binding (fup), tissue:plasma partitioning, and active transporter processes related to excretion (enterohepatic recirculation, and active secretion and reabsorption in kidney).

In addition, in the future we will assess whether *in-vitro* kinetic data can be used to improve the mechanistic model especially with regard to enterohepatic recirculation (MRP 2 and OATP 2B1 e.g.) and kidney transporters (OAT1, OAT2 and OAT4). Currently we have used *in-vitro* apparent permeability data for parameterization using an IVIVE approach. This will help in understanding the feasibility of NAM data for acting as input parameters in PBK models and address the gaps related to such experimental techniques. This harmonised model is developed adhering to all the OECD PBK reporting criteria for which the work is ongoing in T7.3.3 PFAS uncertainty case study.

3.2. Approach

3.2.1 Selection of model compounds

Fig 6 gives an overview of the compounds of interest for this case study perfluorooctanesulfonic acid (PFOS), perfluorooctanoic acid (PFOA), perfluorohexanesulfonic acid (PFHxS) and perfluorononanoic acid (PFNA).

3.2.2 NAM methods

This case study relies on literature data for input of the PBK model with IVIVE-PBK framework. These data are physiological, physicochemical and kinetic data reported in literature. Some of these data are human *in vitro* based data reported on the transfer of PFASs over the intestinal barrier. For calculation of absorption rate constant, an IVIVE (*in-vitro* to *in-vivo* extrapolation) approach was used with data obtained from different cell lines from Janssen et al. (2024). The authors used two models to calculate the transport of PFAS compounds i) human-induced pluripotent stem cells (hiPSC)-derived intestinal epithelial model (IEC) and ii) Caco-2 cells. The apparent permeability (Papp) of PFASs was calculated from the apical to basolateral direction. Papp values were scaled to an absorption rate constant in rat and human using a reported method (Punt et al., 2022) and were incorporated into the PBK models.

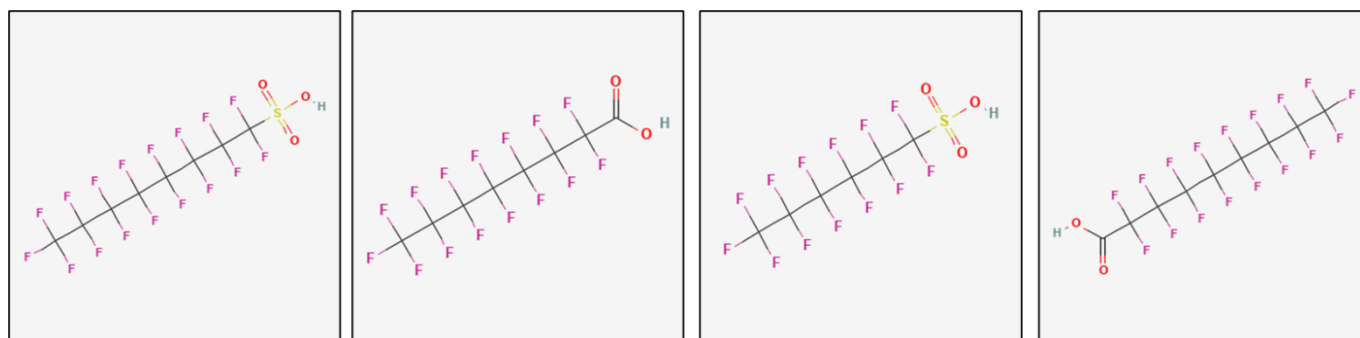


Fig 6: From left to right: chemical structures of PFOS, PFOA, PFHxS and PFNA (PubChem)

3.2.3 PBK modelling

The assumption was to have one generic model to apply to all four PFASs based on extrapolation. The model structure is shown in fig 7. The model is applicable for both rat and human. Physiological parameters for rats were derived from a previously published article (Loccisano et al., 2012). One particular change in the model compared to previously reported models (most of them based on Loccisano et al. (2011)) is that the filtrate compartment is now depending on glomerular filtration from the kidney making it more physiologically relevant. Another big change is that the fraction unbound (fup) has been removed from all equations except for when PFASs are undergoing a particular activity such as being renally excreted and resorbed as only the free fraction of a compound is able to exert a specific activity or effect. A gut lumen has been added to the model to facilitate enterohepatic circulation, and a liver storage compartment has been added to mimic potential sequestration of PFAS to liver fatty-acid binding proteins (L-FABPs) (Han et al., 2021).

The dose was administered directly to the gut compartment with blood flow from the gut responsible for transporting the compound to the liver. In the liver, saturable binding was incorporated, described by maximum binding capacity (Bmax), and affinity constant (kb). This binding phenomenon was elucidated through Michaelis-Menten Kinetics. Compounds like PFOS were found to bind to L-FABP protein, and only the unbound fraction was available for distribution to different organs. The excretion of compounds occurred through urine and feces. In the case of urine, resorption from the kidney was considered through the filtrate compartment, subsequently stored in a storage compartment before being excreted in urine. This model was further validated using data from Tarragona autopsy cohort.

3.2.4 Exposure scenario modelled:

Two exposure scenarios have been modeled for rats and humans for the oral and intravenous absorption routes.

The modelled scenarios were as follows:

Scenario 1: We have built and evaluated PBK models for male and female rats for the four PFASs based on literature reported kinetic data on plasma, urine and when available feces. We have also extracted data of different tissues such as liver and kidney. Different modeling scenarios were built to optimize and evaluate the model. Both oral and intravenous routes were evaluated.

Scenario 2: The evaluated rat PBK models were extrapolated to human models by allometric scaling of the rat parameters to human parameters. Where possible, the allometrically scaled parameters were replaced with human input e.g. for partition coefficients, fraction unbound in plasma and intestinal transfer. Different aspects have been considered with reliability on i) complete allometric scaling and ii) allometric scaling along with human available data for human PBK models. Human exposure scenarios were defined based on literature studies on drinking water exposure and correspondingly measured plasma levels for all four compounds individually. The final model was used to predict the measured plasma levels.

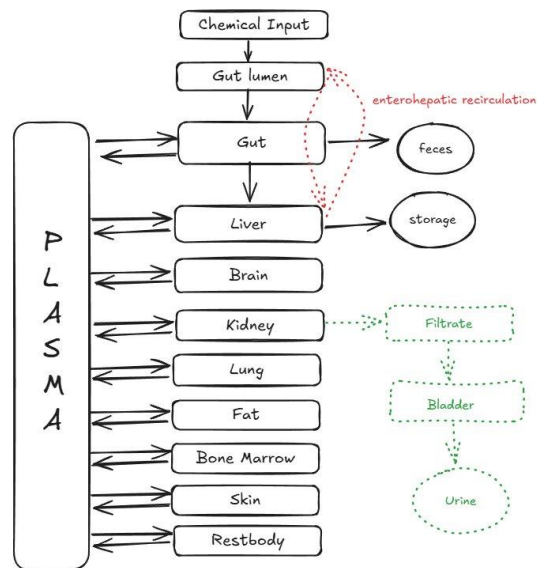


Fig 7: Schematic overview of the generic PBK model for the four PFASs (PFOS, PFOA, PFHxS and PFNA).

3.3. Results

The major findings in this case study are:

The PBK model was evaluated in rats and humans for all four PFAS compounds at various doses using experimental data extracted from published literature. Fig 8 shows the predicted and experimental data for 4 PFASs in rat. It was noted that, for PFOA at a comparable dose, urine excretion was higher in females (Fig. 8C and 8D) compared to males (Fig. 8A and 8B). A similar pattern was observed for PFNA and PFHxS, indicating sex-based differences in the elimination of these compounds. Female rats have a higher excretion via the urine than males have and therefore they have a shorter half-life compared to the males. This higher excretion is amongst others related to the glomerular filtration rate (GFR) of female rats, which is reported to be around 30% higher than that is for male rats (Wen et al., 2020). This same model has been extrapolated to humans to predict plasma levels in human.

The human PBK model was built based on human physiological data from the literature (Brown et al., 1997) for tissue weight and tissue blood flow. Some biochemical parameters were scaled using allometric scaling shown below in equation (eq 1). In this equation K_{human} and K_{rat} refer to rate constants in human and rat, respectively. BW_{human} and BW_{rat} refer to body weight of human and rat, respectively where -0.25 is the allometric exponent. Other parameters like the partition coefficients and the fraction unbound in plasma were derived from literature or kept similar to rat values in case of data unavailability. With adjustments of several kinetic parameters, it was possible to describe the drinking water exposure data with the PBK model predictions. These finalized PBK models for all 4 PFASs show good predictions with steady state achieved in 2-3 years for PFOS and PFOA (manuscript in preparation).

$$K_{\text{human}} = K_{\text{rat}} * (BW_{\text{human}}/BW_{\text{rat}})^{-0.25} \quad \text{eq. 1}$$

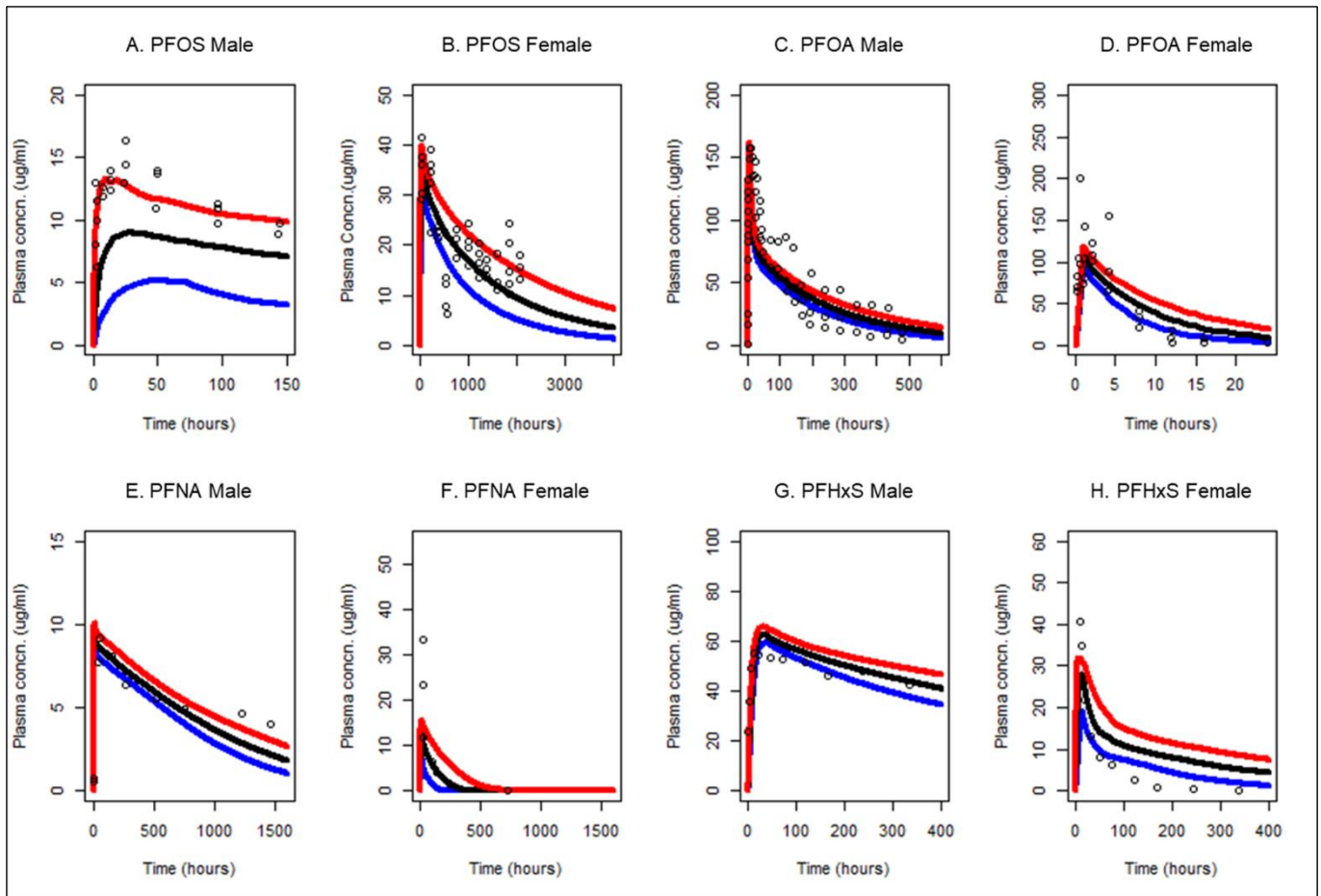


Fig 8.1: Simulated and observed data for all 4 PFAS compounds at different doses: PFOS: 4.2 mg/kg (male: A), 15 mg/Kg (Female: B); PFOA: 25 mg/Kg (male: C and female: D); PFNA: 3 mg/Kg (male: E and female: F); PFHxS: 3 mg/Kg (male: G and female: H). Red line represents 97.5 percentile, black line median and blue line 2.5 percentile. Open circles represent observed data.

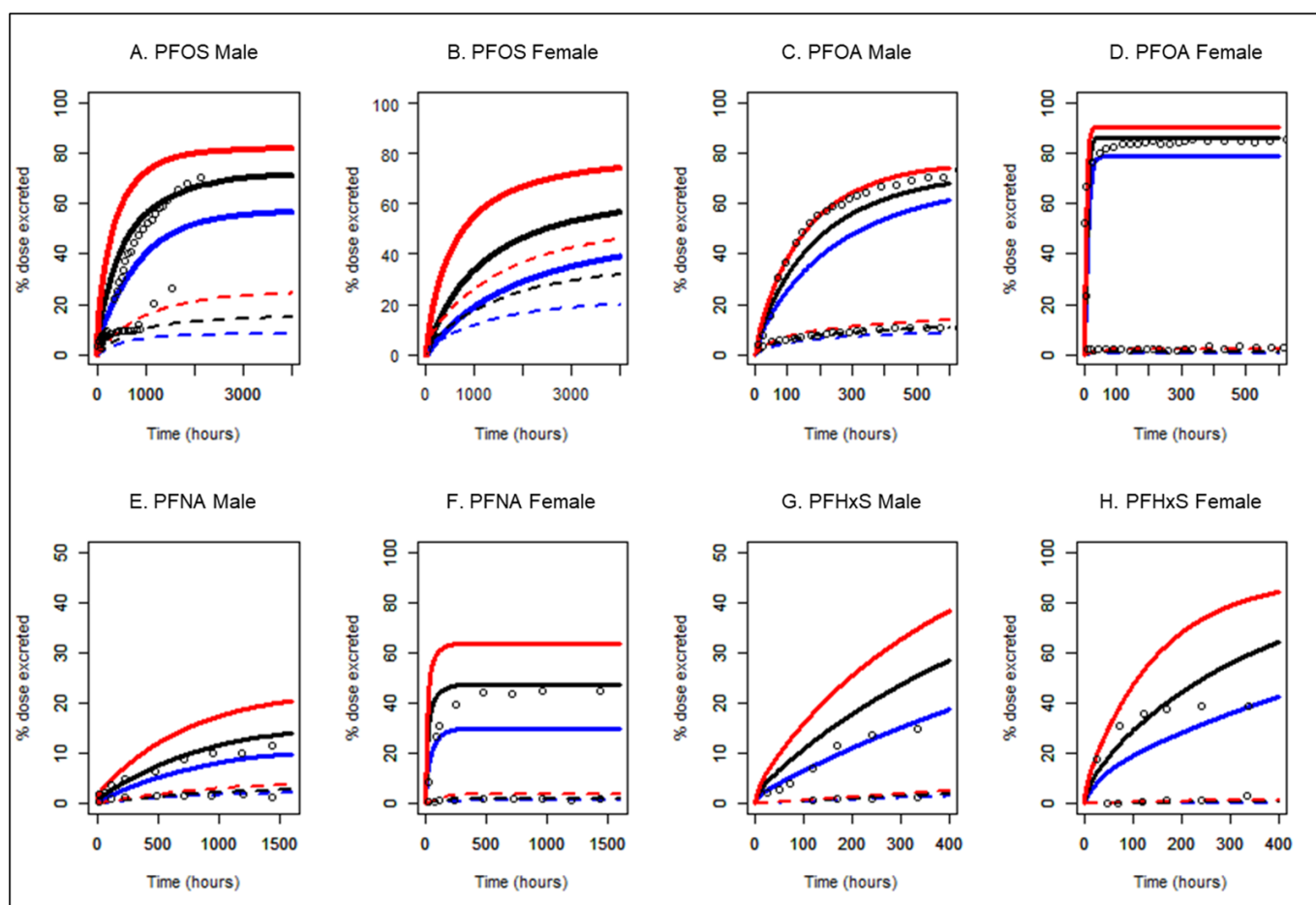


Fig 8.2: Simulated and observed data for all 4 PFAS compounds at different doses: PFOS: 4.2 mg/kg (male: A), 15 mg/kg (Female: B); PFOA: 25 mg/kg (male: C and female: D); PFNA: 3 mg/kg (male: E and female: F); PFHxS: 3 mg/kg (male: G and female: H). Continuous line represents urine and dotted line represents feces. Open circles represent observed data.

3.4. Discussion

The PBK model was successfully evaluated in rats using *in vivo* kinetic data from the literature. Significant differences were observed between males and females, some of which are also seen in humans. The case study highlights the interspecies differences in PFASs, as their ADME parameters vary between rats and humans. This modelling result is in line with the *in vivo* observed half-lives of the PFASs in rats, which are significantly shorter than those found in humans (National Toxicology Program, 2022a, b; Rosato et al., 2024).

The case study further illustrates that simple allometric scaling from rat to human is sometimes insufficient to accurately describe the kinetics of PFASs in humans. This limitation likely arises from the substantial toxicokinetic differences between species—PFASs exhibit half-lives of only hours in rats, compared to years in humans. Knowledge gaps for humans remain due to a lack of reliable *in vivo* kinetic data such as plasma/urine data in time following known exposures. Such data are needed to improve human PBK models and build enough confidence to extrapolate them for sensitive populations. In the future, validated PBK models can be used to calculate daily intake levels for sensitive populations and compare them with the EFSA tolerable weekly intake.

Newly developed harmonized PFAS PBK models will be freely available and accessible through GITHUB once we are ready to publish the manuscript in the coming months.

4. Case study 3 - Integration of Isoform Specific Metabolism into PBK models - example Organophosphates (ISS, ITEM)

4.1 Case study Background and Objectives

Lifestage-specific metabolism in humans refers to the dynamic changes in metabolic processes that occur across various stages of life, including infancy, childhood, adolescence, adulthood, and old age. These variations significantly influence how the body absorbs, metabolizes, and excretes various compounds, including food and feed additives. For example, children may metabolize certain chemicals differently than adults due to their developing organ systems, which can lead to increased susceptibility to potential toxic effects. Understanding these differences is crucial for accurately assessing the risks associated with exposure to these compounds at different life stages.) The age group are defined based on age classification suggested by Eunice Kennedy Shriver National Institute of Child Health and Human Development (NICHD) and the mean age, namely, neonatal, 14 days; infancy, 6 months; early childhood, 4 years; middle childhood, 9 years; and adolescence, 15 years was used to calculate the fractional abundance of the hepatic CYP450 isoforms.

4.1.1 Case study objectives

The case study models the metabolism of organophosphate compounds in different life-stages using CYP specific metabolism data.

4.2. Approach

4.2.1 Selection of model compounds and workflow

Compounds of interest are data-rich organophosphate pesticides, which are commonly found as contaminants in the environment and the food chain (Fig 9). The Fraunhofer PBK model (Nowak et al., submitted) is extended by ontogeny from birth to adulthood as well as female physiology. Ontogeny PBK modelling addresses ADME properties, with a particular focus on enzymatic clearance via cytochrome P450 (CYP)-specific metabolism. Age-specific fractions of CYP enzymes are integrated into the PBK model to accurately reflect the metabolic capacity at different life stages.

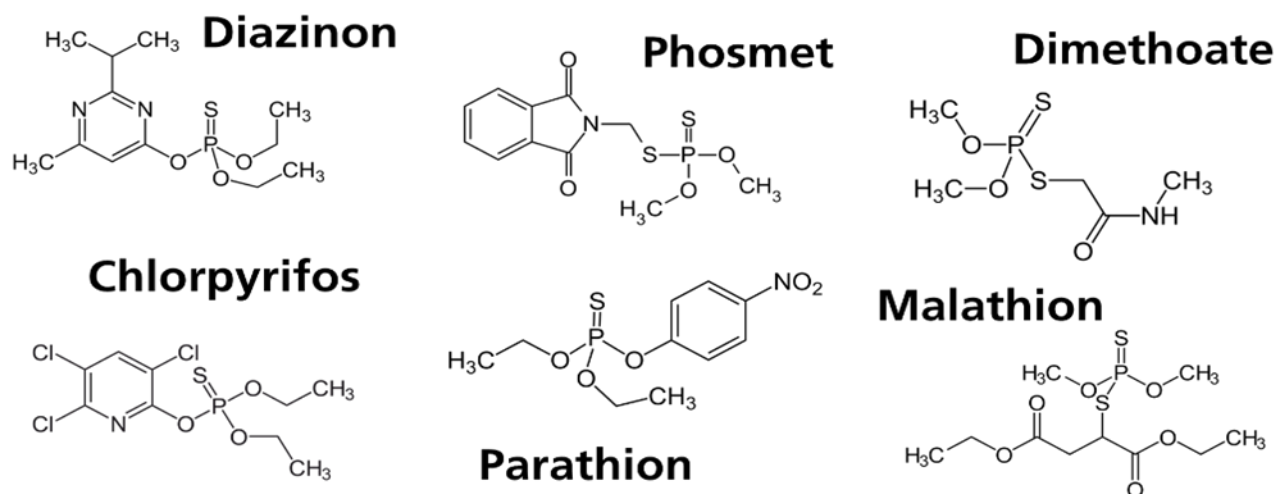


Fig 9: Organophosphate compounds of this case study.

4.2.2 NAM methods

Literature research of liver fractional abundances of CYP enzymes for each life stage had been collected (Achour et al., 2014; Balhara et al., 2022; Pastrakuljic et al., 1997; Thakur et al., 2021) and will be used as the input ontogeny modelling. The age groups are generally classified as neonatal (0–27 days), infancy (28–364 days), early childhood (1 to <6 years), middle childhood (6 to <12 years), adolescence (12 to <18 years), and adulthood (>18 years) as suggested by Eunice Kennedy Shriver National Institute of Child Health and Human Development (NICHD) (Thakur et al., 2021).

In Thakur et al. (2021) the fractional abundance was calculated using the nonlinear regression equation and ontogeny functions provided by Upreti and Wahlstrom (2016) for pediatric groups and weighted mean values of the enzyme abundance in adults from Achour et al. (2014). This data had been updated and recalculated considering the liver content of CYP3A7 reported in Balhara et al. (2022) for neonates and CYP1A1 reported in Pastrakuljic et al. (1997) for adults see Table 1.

Table 1 Liver Protein fraction abundances of CYP450 isoforms in different life stages

| CYP450 isoform | Protein fractional abundances | | | | | |
|----------------|-------------------------------|-----------------------------|----------------------------------------|------------------------------------------|-----------------------------------|--------------------------|
| | Neonatal (0 to 27 days) | Infancy (28 to 364 days) | Early childhood (1 to < 6 years) | Middle childhood (6 to < 12 years) | Adolescence (12 to < 18 years) | Adulthood (>18 years) |
| CYP1A2 | 1.4% | 4% | 6% | 7% | 8% | 10.0% |
| CYP2A6 | 9.1% | 11% | 9% | 9% | 9% | 6.9% |
| CYP2B6 | 7% | 7% | 6% | 5% | 5% | 4.1% |
| CYP2C8 | 7% | 9% | 8% | 7% | 7% | 5.8% |
| CYP2C9 | 18.2% | 25% | 21% | 20% | 19% | 15.7% |
| CYP2C19 | 0.7% | 4% | 4% | 4% | 4% | 2.8% |
| CYP2D6 | 4.9% | 5% | 4% | 4% | 4% | 3.2% |
| CYP2E1 | 9.1% | 19% | 20% | 20% | 19% | 16.6% |
| CYP3A4 | 4.9% | 9% | 16% | 18% | 20% | 23.9% |
| CYP3A5 | 7.7% | 7% | 6% | 6% | 5% | 4.4% |
| CYP3A7 | 30% | | | | | 2.30% |
| CYP1A1 | | | | | | 0.26% |
| CYP2C18 | | | | | | 0.10% |
| CYP2J2 | | | | | | 0.30% |
| CYP3A43 | | | | | | 0.51% |
| CYP4F2 | | | | | | 2.90% |

All the metabolic data of interests on several Organophosphate pesticides (OPTs) (Diazinon, Malathion, Chlorpyrifos, Parathion, Dimethoate and Phosmet) were collected after an extensive literature research.

The isoform specific metabolism data with Intrinsic Clearance (CLi) and Vmax calculation for each CYP450 isoform had been determined using single recombinant enzyme (CYP2B6, 2C8, 2C9, 2C19, 3A4, 3A5, 3A7, 2D6, 1A2, 1A1, 2E1, 2A6 and 2C18). The kinetic curves for the CYPs metabolically active had been obtained from at least three replicates quantifying the toxic metabolite formation (-oxon) using two different methods the AChE inhibition (Diazinon, Malathion, Chlorpyrifos, Parathion and Dimethoate) and an HPLC DAD method (Chlorpyrifos, Parathion and Phosmet) (Buratti et al., 2003; Foxenberg et al., 2007; Santori et al., 2020).

The curve fitting and the kinetic parameters (Km, Vmax and CLi) were calculated for each CYP450 active isoform mainly using the software GraphPad Prism™. Vmax and Km for each CYP contributing to the metabolism are used as input and the intrinsic clearance is calculated by the following equation.

$$Cl_{int} = \frac{V_{max}}{K_m}$$

Using the Cl_{int} (for enzymatic high affinity phase) and V_{max} (for enzymatic low affinity phase) data collected, the % contribution to the metabolism was determined for each CYP450 isoform in the different life stages multiplying the single isoform fractional abundance for the own kinetic parameters (Fig 10).

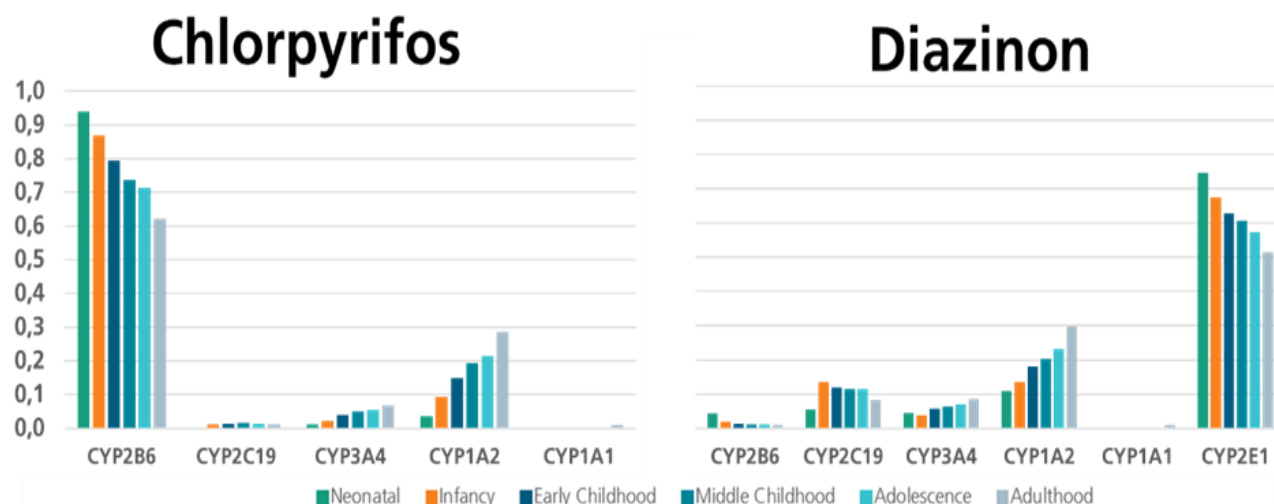


Fig 10: Contributions of different CYP isoforms in the hepatic metabolism of a developing human in the example of chlorpyrifos, diazinon (high affinity phase).

Differences between the two enzymatic affinity phases were evidenced in all different life stages as exemplified in the table below for Chlorpyrifos

Table 2 Chlorpyrifos. Percentual contribution to the oxon formation of each active CYP450 isoform: enzymatic high affinity phase (in orange) and low affinity phase (in green).

| | Neonatal (0 to 27 days) | Infancy (28 to 364 days) | Early childhood (1 to < 6 years) | Middle childhood (6 to < 12 years) | Adolescence (12 to < 18 years) | Adult >18 years |
|----------------|----------------------------|-----------------------------|-------------------------------------|---------------------------------------|-----------------------------------|--------------------|
| Isoform | | | | | | |
| CYP2B6 | 94.0 | 86.8 | 79.3 | 73.6 | 71.3 | 62.2 |
| CYP2C19 | 0.2 | 1.3 | 1.3 | 1.5 | 1.4 | 1.1 |
| CYP3A4 | 1.2 | 2.1 | 4.0 | 5.0 | 5.4 | 6.9 |
| CYP3A5 | 0.6 | 0.5 | 0.4 | 0.5 | 0.4 | 0.4 |
| CYP3A7 | 0.4 | 0.0 | 0.0 | 0.0 | 0.0 | 0.04 |
| CYP1A2 | 3.5 | 9.3 | 14.9 | 19.4 | 21.4 | 28.5 |
| CYP1A1 | | | | | | 1.0 |
| CYP2B6 | 48.1 | 41.9 | 43.8 | 23.1 | 21.6 | 16.3 |
| CYP2C19 | 1.1 | 5.7 | 1.9 | 4.4 | 4.1 | 2.7 |
| CYP3A4 | 25.8 | 41.4 | 52.0 | 63.7 | 66.4 | 72.6 |
| CYP3A5 | 10.9 | 8.6 | 1.8 | 5.7 | 4.4 | 3.5 |
| CYP3A7 | 13.1 | 0.0 | 0.0 | 0.0 | 0.0 | 0.58 |
| CYP1A2 | 1.0 | 2.4 | 0.4 | 3.2 | 3.4 | 3.9 |
| CYP1A1 | | | | | | 0.5 |

CYP ontogeny is considered by the calculated fraction of CYP enzymes per life stage and scaled to CYP P450 content per gram liver (Wilson et al., 2003).

For the comparison of life stage modelling, the example of chlorpyrifos is chosen. Lifestages include their respective underlying anatomy (body height/weight, surface area), which translates to relevant physiology such as organ volumes, blood flows and protein content by ontogeny equations (e.g. Beaudouin et al. (2010)). The PBK model of chlorpyrifos is validated for available data for an adult male human (Timchalk et al., 2002) and the same exposure scenario (2 mg/kg oral ingestion together with a volume of 100 ml) is used for life stages of interest.

4.3. Results

PBK model results are exemplarily shown for compound Chlorpyrifos and CYP450 1A2, 2B6, 2C19, 3A4, 3A5, 3A7. Preliminary results from the PBK model indicate that there are notable differences in kinetics across life stages and between genders for the same exposure scenario. In males time dependent differences in clearance with highest relative metabolic activity in early childhood are seen (Fig 11). The female PBK model also predicts the early childhood to be the most relative metabolic active life stage. Interestingly, there is a gender specific difference in the infant model with female blood concentration reaching levels comparable to adolescence and adulthood stage.

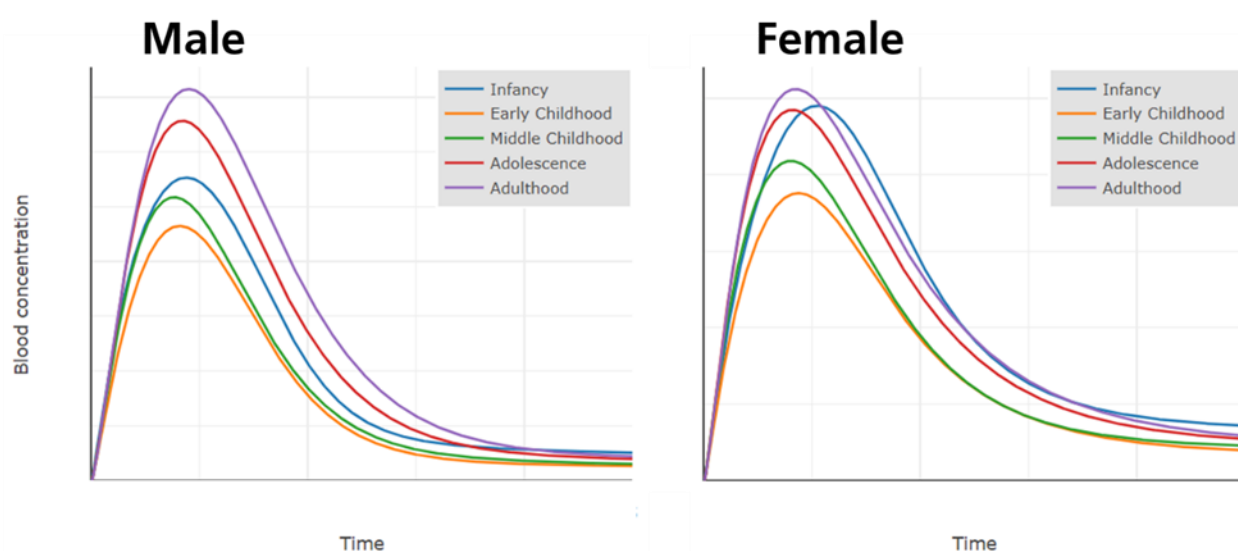


Fig 11: Exemplary blood concentration curves of chlorpyrifos (2 mg/kg) for the same exposure in different life stages.

Preliminary model kinetics for chlorpyrifos in different life stages are presented in Table 3. Gender differences are seen within life stages, especially in later life stages closer to adulthood such as middle childhood and adolescence. All other compounds and more detailed data will be generated and published in a peer reviewed publication.

Table 3: Model kinetic parameters of different life stages for male and female humans.

| Lifestage | Gender | Cmax (ng/ml) | Tmax (h) | AUC (ng*h/ml) |
|------------------------|--------|--------------|----------|---------------|
| Infancy (0.5 years) | Male | 2.7 | 0.88 | 5.1 |
| | Female | 2.5 | 1.05 | 5.6 |
| | Male | 2.3 | 0.82 | 3.9 |

| | | | | |
|---------------------------------------|--------|-----|------|-----|
| Early Childhood (4 years) | Female | 1.9 | 0.88 | 3.9 |
| Middle Childhood (9 years) | Male | 2.6 | 0.77 | 4.4 |
| | Female | 2.1 | 0.81 | 4.3 |
| Adolescence (15 years) | Male | 3.3 | 0.84 | 6.0 |
| | Female | 2.4 | 0.82 | 5.2 |
| Adulthood (20 years) | Male | 3.6 | 0.90 | 6.8 |
| | Female | 2.6 | 0.85 | 5.6 |

4.4. Discussion

Life stage dependent modelling is needed in case of risk assessment for most susceptible human populations (Testai et al., 2021). Gender specific differences in developmental changes at lifestages as well as during development in general give insights into potentially sensitive timepoints.

The reported case study evaluates realistic exposure scenarios for different human life stages, focusing on the liver metabolism, modeling these scenarios within the ontogeny PBK framework. This analysis aims to compare exposure metrics and kinetic profiles for plasma and tissues of interest, providing valuable insights into the exposure risks faced by potentially susceptible populations, such as infants and children. Ultimately, this research will enhance our understanding of how life stage-specific hepatic metabolism influences the health risks associated with exposure to organophosphate pesticides and similar compounds.

Starting from the adolescence at age 15, the model's tissues and basic underlying physiology begin to be fully developed. Body height's steep increase during childhood starts to plateau during adolescence, this dynamic is also seen in body weight and volumes of main tissues and organs. However, some kinetics and metrics (e.g. microsomal protein per gram liver (MPPGL), cardiac output and the glomerular filtration rate (GFR) of the kidney) remain changing in their value throughout the life span of human beings. The comparison of earlier life stages to adulthood are substance and exposure specific.

Ontogeny modelling works, as PBK modelling in general, with assumptions. In the case of data gaps for physiology changes these were tried to be defined in a profound manner. Life stage specific metabolism and PBK modelling provided first promising results with the assumptions taken. Whether these reflect the *in-vivo* situation in a fairly good way should be further validated with available data for all life stages and genders. *In-vivo* blood/plasma data for all life stages are often missing, model validation will be done with available metrics such as amounts excreted in urine of exposed population data. Further case studies, e.g. on pyrethroids pesticides, are in preparation at PARC in order to generate a broader understanding and expand the previously limited application domain.

5. Case study 4 - Develop a tiered testing for inhalable compounds (INERIS, ITEM, AUTH)

5.1 Case study Background and Objectives

Inhalation is a primary route for chemical exposure, yet it's poorly understood due to challenges in traditional toxicology, including complex equipment needs and limitations of animal models. NAMs like in vitro models (e.g., ALI models, lung organoids) offer insights into chemical absorption and toxicity but face constraints due to experimental conditions that may overlook physiological variability. Effective regulatory use of these models requires ensuring human-relevant exposure conditions, suitable cell models, and relevant read-outs at appropriate times. PBK modeling integrates in vitro data, accounts for individual variability, and predicts the fate of chemicals through ADME. Accurate experimental or predicted data are crucial for PBK models to reduce uncertainty and enhance risk assessment decisions. This work aims to evaluate in vitro lung barrier models to predict absorption, intracellular accumulation, and permeation of chemicals upon exposure.

5.2. Approach

5.2.1 Identification of the current gaps

Developing predictive PBK models requires accurate ADME parameterization and a detailed understanding of human respiratory physiology.

5.2.1.1 Physiological Gaps

Generic models often simplify the lung as a single organ (Tebby et al., 2020), while it consists of two functional zones: the conducting airways and the respiratory zone, crucial for gas exchange and xenobiotics absorption. There is significant variability among individuals.

5.2.1.2 Absorption Gaps

Data on inhalation absorption is limited due to complexities like regional deposition and perfusion. More research is needed on factors influencing absorption.

5.2.1.2 Experimental Gaps

In vitro systems face variability and uncertain exposure, limiting toxicity assessment. Accurate intracellular measurement is essential for developing biokinetic models and QIVIVE. Chemical behavior in assays is influenced by factors like vaporization and binding, with biokinetic models aiding in determining dose availability.

5.2.2 Experimental models tested

Inhaled chemical transport through the epithelial barrier is crucial for determining systemic absorption. Current tools fail to accurately predict permeability, necessitating specialized experimental assays. Various models have been assessed to balance predictive ability and cost.

Table 4: Experimental model tested in the case study

| Model | Characteristics | Barrier properties | Complexity and cost |
|--------------|---------------------------|----------------------------------------|---------------------|
| PAMPA | Lipidic membrane | Passive transport | - |
| Calu-3 cells | Lung adenocarcinoma cells | Tight junctions, mucus secretion (ALI) | + |

| | | | |
|----------------------|------------------------------------------|--------------------------------------------------|-----|
| h-AELVi cells | Primary human bronchial epithelial cells | Tight junctions, no data on secretory capacities | +++ |
|----------------------|------------------------------------------|--------------------------------------------------|-----|

5.2.2.1 PAMPA

PAMPA (Parallel Artificial Membrane Permeability Assay) is a convenient, low-cost method that mimics cell membranes to simulate gastrointestinal tract permeability, aiding in understanding chemical absorption (Di et al., 2003; Kansy et al., 1998; Wohnsland and Faller, 2001) Unlike traditional cell-based assays, PAMPA is quick and affordable, measuring the rate at which compounds pass through the membrane to offer insights into absorption and distribution properties.

5.2.2.2 Calu-3

Calu-3 cells are derived from lung adenocarcinoma and are used in permeability studies due to their formation of tight junctions and high transepithelial electrical resistance, mimicking human airway epithelium. These cells can be cultured in both liquid-liquid interface (LLI) or an air-liquid interface (ALI)..

5.2.2.3 h-AELVi

h-AELVi cells are derived from human alveolar epithelium through lentiviral immortalization. Unlike the cancerous Calu-3 cells, h-AELVi cells provide a more physiological model for studying alveolar permeability.

5.2.2.4 Experimental setup

For air liquid interface culture (ALI), Calu-3 or h-AELVi cells were seeded onto Transwell® inserts (12-well, 0.4 µm pore size, polyester membrane, Costar® Corning Incorporated) at a density of 5x10⁴cell/cm² and 1 x10⁵ cellules/cm², respectively. After 48 hours, the apical medium was aspirated to establish ALI conditions, and cells were cultured for 14 days with basolateral medium (1500 µL) replenishment every 48 hours (Figure 1). Prior to the permeability assay, epithelial barrier integrity was assessed via transepithelial electrical resistance (TEER) measurements. Test solutions were prepared in cell culture medium at non-cytotoxic concentrations (1 and 10 µM). For permeability assay in apical to basolateral (A-B) direction, the apical chamber was loaded with 500 µL of test solution, while the basolateral compartment received 1500 µL of medium. Aliquots (500 µL) were sampled from the basolateral side at 30, 60, 90, 120 minutes, and 22 hours over a 24-hour period. Upon completion of the incubation, 500 µL samples were collected from both apical and basolateral chambers, and cells were trypsinized to quantify cellular uptake.

For liquid liquid interface culture (LLI), cells were seeded onto Transwell® inserts (12 wells, 0.4 µm pore size, Corning) at a density of 1 x10⁵ cellules/cm² and maintained for 7 days. Both apical (500 µL) and basolateral (1500 µL) media were changed every 48 hours. TEER measurements were conducted to verify monolayer integrity before the permeability assay. The transport study was performed in the apical-to-basolateral (A-B) direction, with 500 µL of test solutions added to the apical compartment and 1500 µL of medium to the basolateral side. Samples (500 µL) were collected from the basolateral compartment over a duration of 2 hours, at intervals of 30-, 60-, 90-, and 120-min. Post-incubation, 500 µL samples were obtained from both apical and basolateral chambers, and cells were trypsinized for cellular uptake quantification.

5.2.2.5 Papp Calculation

The apparent permeability is calculated as follows:

$$P_{app} = \frac{(V_{basal} \cdot dC_{basal})}{dt \cdot Area \cdot C_{o,apical}}$$

Papp = Apparent permeability

dQ/dt = Change in volumetric flow rate over time in seconds.

A = Area of surface in contact with membrane absorption

Co = Initial concentration

5.2.3 Chemicals

5.2.3.1 Chemical Selection

Chemicals are selected based on diverse physicochemical properties to ensure model robustness, covering a wide range of characteristics.

Table 5: Compounds selection based on review of available *in vitro* and *in vivo* ADME studies (PubChem, Chempider or htk databases (Wetmore et al., 2015; Williams et al., 2017))

| Name | CAS | Henry Constant | Mass molar | pKa | logPow | logKoa | Water solubility | Vb | BP | fu |
|-------------------------------|-------------|-----------------------------------------------------------------------------|------------|---------------------------------------------|--------|--------|------------------|----------------------|---------|---------|
| | | atm .m ³ .mol ⁻¹ | g/mol | | | | mg/L | cm ³ /mol | | |
| Thymol | 89-83-8 | 3.50.10 ⁻⁶ | 150 | 10.6 | 3.3 | | 900 | 154 | No data | No data |
| Propranolol | 525-66-6 | 1.43.10 ⁻⁹ predicted ^a | 259 | 9.45 | 3.48 | 8.40 | 61.7 | 237 | 0.86 | 0.33 |
| Sumatriptan | 103628-46-2 | 4.47.10 ⁻¹⁴ ; 2.02.10 ⁻⁸ predicted ^a | 295 | pKa1 : 11.2 4 pKa2 : 9.54 | 0.93 | 9.17 | 40.3 | 238 | 1.03 | 0.83 |
| Hippuric acid | 495-69-2 | 4.32.10 ⁻¹⁰ predicted ^a | 179 | 3.07 | 0.31 | 8.09 | 3750 | 141 | No data | No data |
| Mono (2-ethylhexyl) phthalate | 4376-20-9 | 1.64.10 ⁻⁹ predicted ^a | 278 | 3.37 | 4.93 | 10.4 | 245* | 256 | No data | No data |

Vb: Molar volume; BP: Blood to plasma partition ratio, fu: Fraction unbound (fraction not bound to human plasma proteins), aCompTox

5.2.3.2 Nominal concentration Selection

Cytotoxicity assays using resazurin and LDH release were conducted to assess cell barrier disruption affecting permeability. Tested on h-AELVi and Calu-3 cells with five chemicals, no cytotoxicity was observed at 0.1 to 10µM concentrations, allowing permeability studies at these tested concentrations.

5.2.4 Analytical Methods

Chromatographic/Mass Spectrometric Conditions.

Optimized methods for accurate detection and quantification were developed for each compound, using MRM transitions, collision energies, and polarity settings in chromatography-tandem mass spectrometry (See Table 4).

Table 6: Chromatographic and Mass Spectrometric Conditions for all the compounds. The methods are validated for all compounds.

| Compound Analysis | Technique | Column | Mobile Phase | Flow Rate | Column Temp | Ionization Mode |
|-------------------|-----------|--------|--------------|-----------|-------------|-----------------|
|-------------------|-----------|--------|--------------|-----------|-------------|-----------------|

| | | | | | | |
|---------------|----------|-----------------------------------------------|------------------------------------------------|-------------|------|-----------------------------------------------------------------|
| Thymol | GC-MS/MS | DB-5 MS | N/A (Gas Phase, Ultra-pure helium 99.999%) | 1.3 mL/min | N/A | Electron Ionization (EI) - 70 eV |
| Propranolol | LC-MS/MS | 1.7 um Fortis H ₂ O Size: 50x2.1mm | Aqueous and Acetonitrile with 0.1% Formic Acid | 0.35 mL/min | 40°C | Electrothermal Ionization 3700 V(Positive) |
| Sumatriptan | LC-MS/MS | 1.7 um Fortis H ₂ O Size: 50x2.1mm | Aqueous and Acetonitrile with 0.1% Formic Acid | 0.35 mL/min | 40°C | Electrothermal Ionization 3700 V (Positive) / 3000 V (Negative) |
| Hippuric acid | LC-MS/MS | 1.7 um Fortis H ₂ O Size: 50x2.1mm | Aqueous and Acetonitrile with 0.1% Formic Acid | 0.35 mL/min | 40°C | Electrothermal Ionization 3700 V (Positive) / 3000 V (Negative) |
| MEHP | LC-MS/MS | 1.7 um Fortis H ₂ O Size: 50x2.1mm | Aqueous and Acetonitrile with 0.1% Acetic Acid | 0.4 mL/min | 40°C | Electrothermal Ionization 3000 V (Negative) |

The LOQ for the different compounds are: Sumatriptan 1ppb, Hippuric 1ppb, MEHP 0.1ppb, Propranolol 0.1ppb, Thymol 0.1ppb

5.3. Results

5.3.1 Permeability assays

The permeability formula has limitations as it doesn't account for chemical loss due to plastic binding, cell sequestration, evaporation, and abiotic degradation, resulting in decreased apparent permeability.

Secondly, the permeability value is subject to variation depending on the duration of the sampling period. It has been determined that, in the event of the kinetic permeability not being linear, the Papp value calculated using earlier timepoints will exceed the value calculated using later timepoints.

In order to address these issues, a series of dedicated assays were performed to characterize and evaluate the fractions lost due to plastic or protein binding. These results were then confronted with the mass balance estimated from the experiments.

The initial concentration in the apical well was then corrected using chemical loss fractions that had been determined analytically from the mass balance. A comparison of assays such as Caco2 (from literature), Calu3 (ITEM and INERIS), h-AELVi cells, and PAMPA (Pastrakuljic et al., 1997) for five compounds showed PAMPA's lower permeability for ionizable compounds, suggesting transporter involvement.

5.3.2 Development of the Biokinetic Model

Current *in vitro* cell systems face limitations due to interlaboratory variability and insufficient data on intracellular chemical concentrations, hindering biokinetic modeling and QIVIVE development. Insights into chemical fate, particularly for permeability assays, are essential to refine exposure estimates and enable extrapolation. The proposed model, relying on VCBA (Comenges et al., 2017) and VIVD (Fisher et al., 2019), aims to bridge these gaps by simulating cellular chemical concentrations and accounting for partitioning and binding effects. A sensitivity analysis identified influential parameters like logP, free fraction, pKa, medium pH, and temperature, enhancing prediction precision.

5.3.2.1 Model Description

The model is divided into three parts: the apical side (medium, plastic walls, air), the cell line (mitochondria, lysosomes, microsomes, remainder of the cell), and the basolateral side (medium, plastic, air). It includes connections between plastic and air concentrations on the apical and basolateral sides (Fig 13).

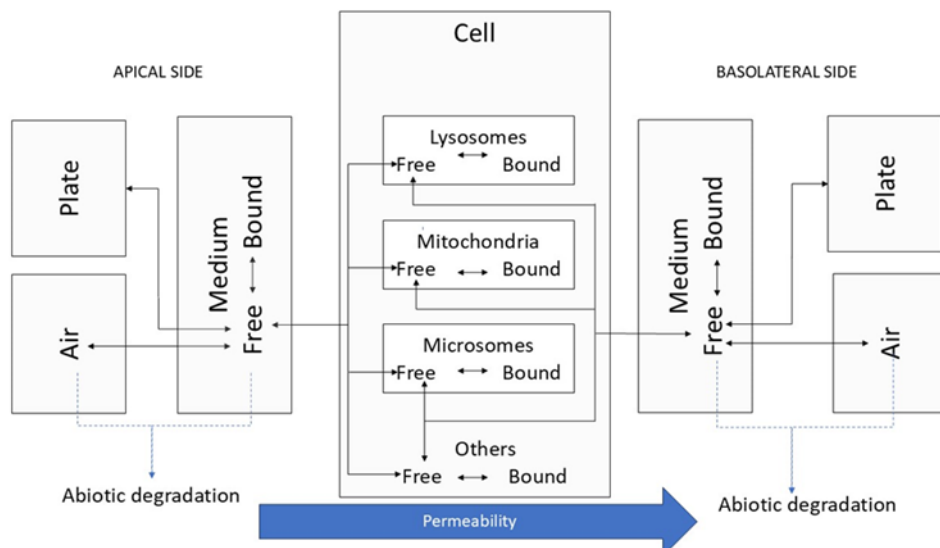


Fig 13: Overview of the biokinetic model proposed for permeability assessment

5.3.2.2 Sensitivity Analysis

Sensitivity analysis performed on parameters affecting cell and medium concentrations in a simulated Transwell® plate identified six key parameters using Morris's method (Morris, 1991) at three timepoints: 0.1, 1, and 12 hours. Enhancing determination of logP, free fraction, pKa, medium pH, and temperature would lead to precise predictions.

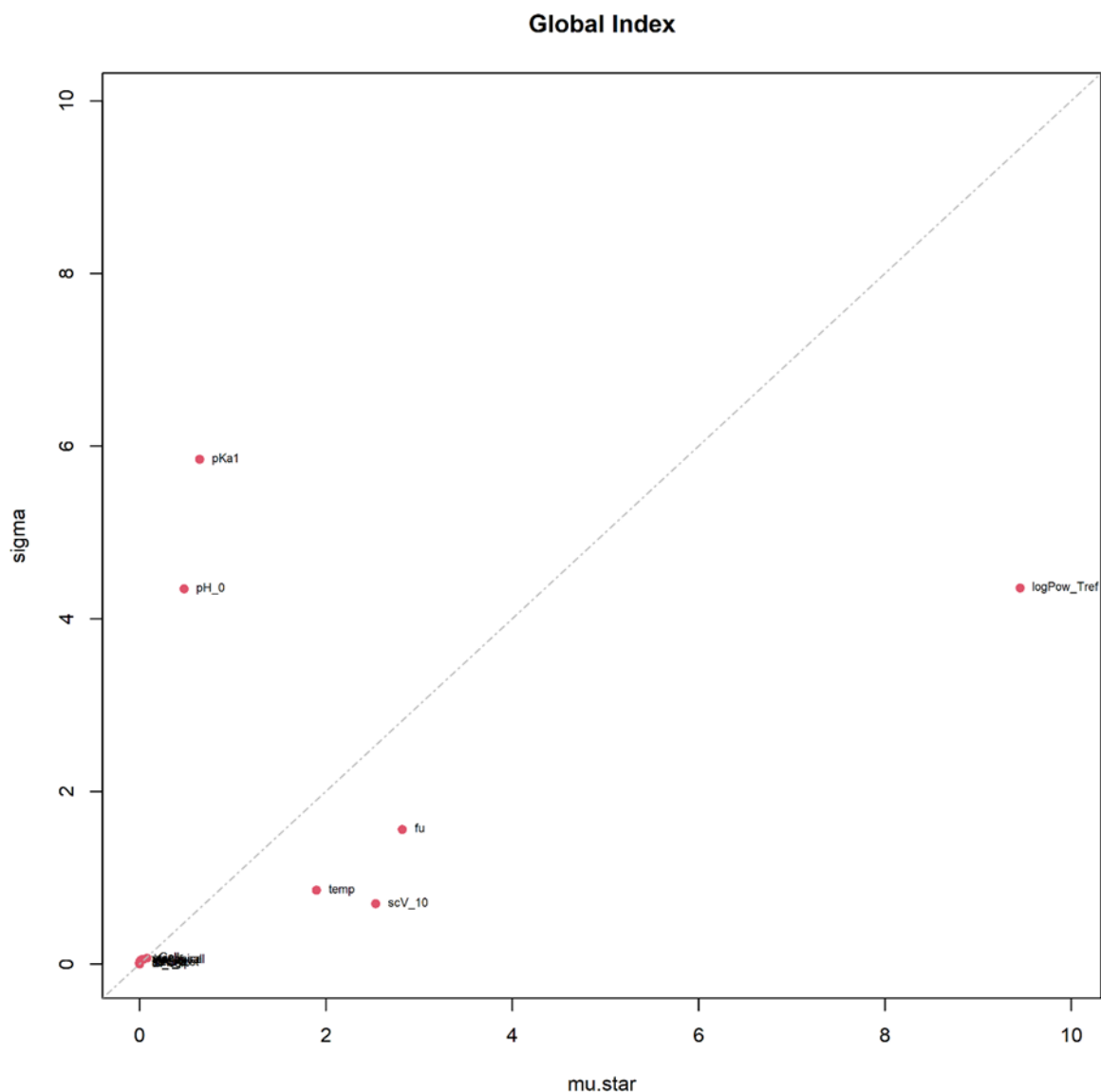


Fig 14: Global sensitivity analysis using Morris's method

5.3.3 PBK Model

At Fraunhofer ITEM, the lung-based model PBKIt(c) simulates inhalation exposure (Tepper and Johnstone, 2018) using 1000 μg of dry powder with 5 μm particles for five compounds. Minimal variations in plasma kinetic curves occurred for four compounds, but significant differences for ionizable compounds in PAMPA assay inputs compared to cell-based assays at physiological pH 7.4. A tiered testing strategy starts with 'Tier 0,' assuming no intrinsic hepatic clearance, and progresses to 'Tier 1,' incorporating *in vitro* hepatic clearance data, affecting elimination kinetics.

The PAMPA assay shows smaller Papp values compared to barrier organs, indicating passive absorption doesn't fully explain permeability for the tested compounds, especially ionizable hippuric acid. Hippuric acid absorption varies significantly, from h-AELVi (1E-4 cm/s) to PAMPA (1E-9 cm/s), due to its ionizable nature at pH 7.4. *In vivo* studies suggest secretory transporters enhance their excretion, also seen in Caco-2 cells. Calu-3 and Caco-2 results align, supporting Sabinovska et al. (2020) that a tiered testing strategy can use either value for absorption estimation. Minimal differences between Tier 0 (glomerular filtration) and Tier 1 (+hepatic clearance) are due to low clearance or low unbound plasma fractions.

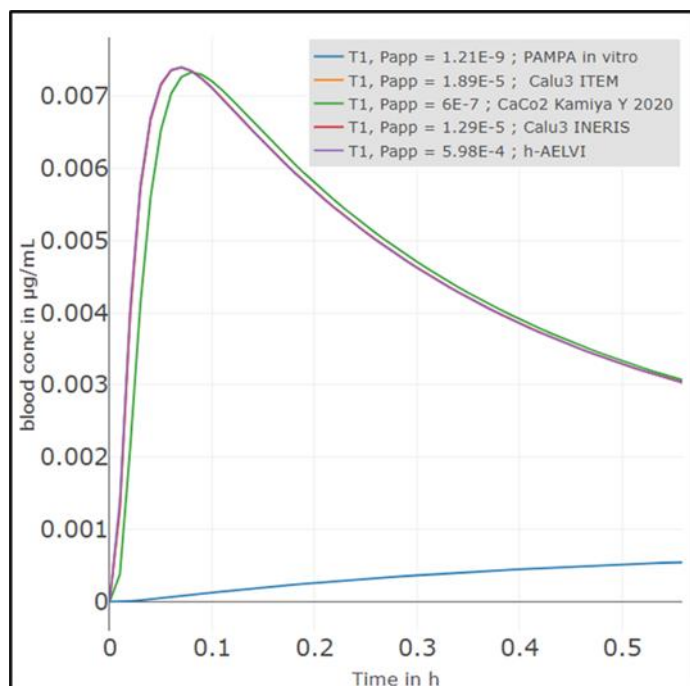


Fig 15: Hippuric acid Tier 1 approach, shows variation in plasma kinetic curve for PAMPA assay and all other cell-based assays.

5.4 Conclusion

Accurate assessment of lung model permeability requires considering free available chemical fraction rather than nominal concentration alone. Nominal concentration doesn't account for processes like binding, adsorption, volatilization, metabolism, and degradation, influencing chemical availability. Chemicals, especially lipophilic ones, can adsorb plastic walls, reducing freely available concentration. Binding to proteins further decreases permeability availability, and rapid metabolism can lead to overestimation. Integrating chemical loss mechanisms through computational modeling provides realistic permeability assessments, facilitating new assay designs and extrapolation to human populations.

6. Case study 5 - The role of the blood brain barrier in PBK models (BfR, IISPV)

6.1 Case study Background and Objectives

Blood-brain-barrier (BBB) is a selective semi permeable membrane restricting the passage of most chemicals by acting as a barrier between circulating fluid and brain's extracellular fluid. BBB plays a critical role in PBK models especially when we want to understand the kinetics of chemicals that causes neurotoxicity. Recent studies have implicated towards role of long-acting compounds like perfluorinated compounds (PFAS) (Bharal et al., 2024) and fast metabolizing compounds like insecticides (Neylon et al., 2022) in affecting brain functions and causing dementia, Alzheimer, memory loss etc.

The objective of this case study is to i) conducting *in-vitro* studies using BBB cell lines to calculate passive and active permeation, ii) incorporate QIVIVE approach into brain PBK for parameterizing the biochemical parameters related to brain compartments, and iii) explore the risk assessment for neurotoxic chemicals like PFOS, PFOA, permethrin, cyfluthrin and chlorpyrifos by developing a brain specific PBK model using in-vitro data. The model developed here will be further used in T 6.2 for extending to other class of chemicals for human health risk assessment.

6.2. Approach

6.2.1 Describe model compounds

Five model compounds have been used: perfluorooctanesulfonic acid (PFOS), perfluorooctanoic acid (PFOA), chlorpyrifos, permethrin and cyfluthrin (Fig 15).

6.2.2 Described NAM methods

Blood brain barrier cell lines called as immortalized human capillary microvascular endothelial (HCMEC/D3) were used to calculate apparent permeability (Papp) from apical to basolateral (A-B) and basolateral to apical (B-A) for different compounds. Active transport was measured using P-GP expression. Other tests like cell viability and genetic expression using RT-PCR were also conducted.

6.2.3 Describe analytical methods

Bidirectional permeability was calculated using GC-ECD. Analysis was carried out by CSIC, Barcelona, Spain in collaboration with Prof. Joan O. Grimalt. Detail about analysis for insecticides have already been published in article (Deepika et al., 2022). Similar types of methods have been used for quantifying PFOS and PFOA.

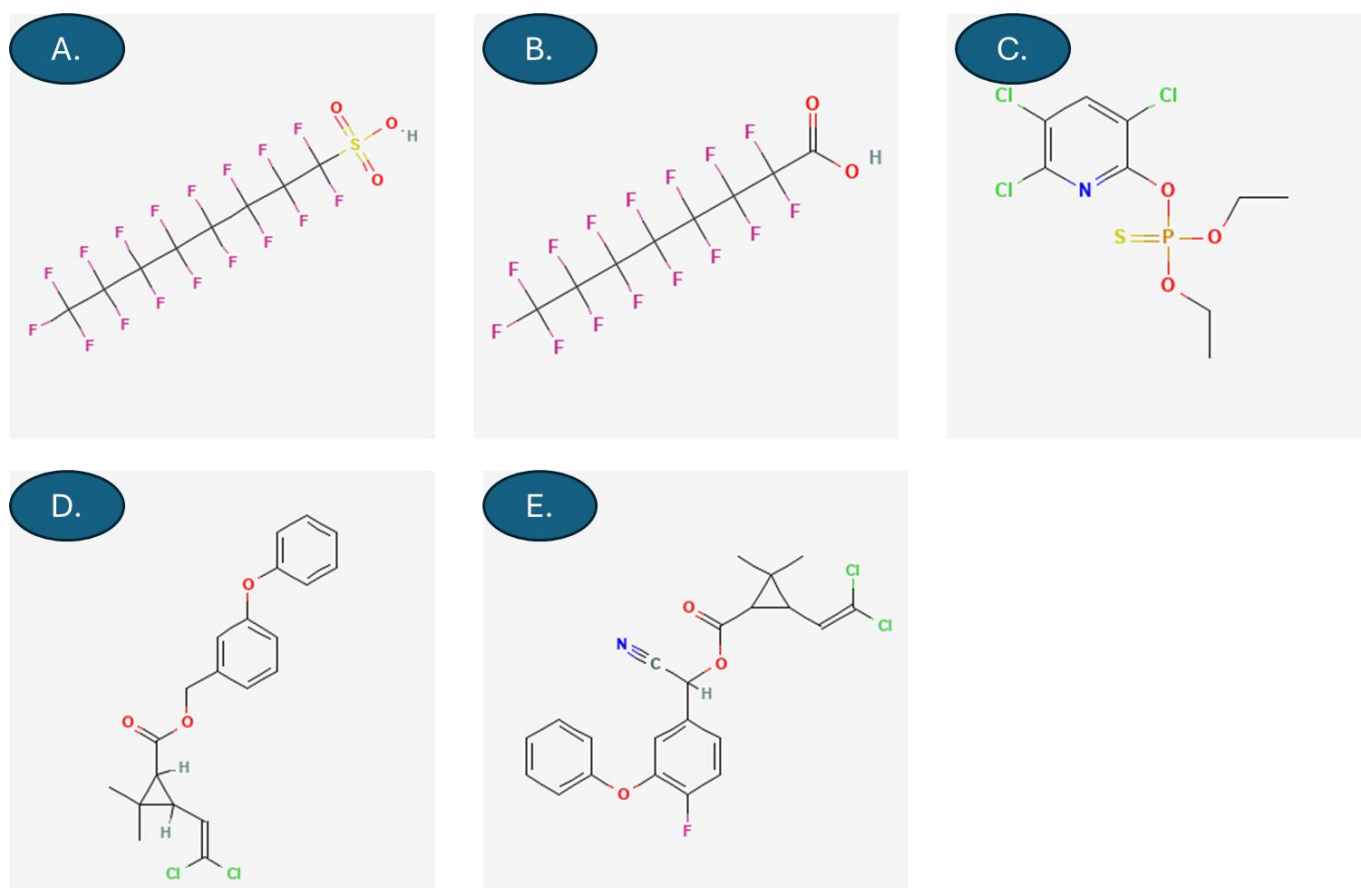


Fig 15: Model compounds used for BBB case study: A) PFOS, B) PFOA, C) Chlorpyrifos, D) Permethrin, and E) Cyfluthrin.

6.2.4 Description of PBK model structure and assumptions; source of physiological data (or provide reference)

Brain PBK model was developed only for PFAS compounds with the possibility in future to extend it for insecticides and other chemicals. Validated PBK model from CS2 for rat and human has been taken as the base for extending the same structure to brain PBK. Brain compartment has been divided further into five subcompartments (Fig 16): hippocampus, cortex, rest of brain, brain blood and cerebrospinal fluid. Physiological parameters for these compartments have been extracted from published article (Delgado-Gonzalez et al., 2015; Zakaria and Badhan, 2018). Some biochemical parameters were calculated using in-vitro data with IVIVE like Papp while others were extracted from literature. Fraction unbound (fu) was considered similar for plasma and brain compartments due to lack of data. A CV (coefficient of variation) of 30% was applied for human parameters to incorporate uncertainty arising while moving from one species to another.

Table 7: Physiological parameters of rat and human for the blood brain barrier PBK Model

| Parameters | Rat | Human |
|-------------------------------------------------------------|-------|---------|
| Organ volume as a fraction of total body weight (Kg) | | |
| Fraction of volume of brain^a | | |
| Fhipp | 0.052 | 0.00378 |
| Fcr | 0.347 | 0.4 |

| | | |
|----------------------------------------------|---------|---------|
| Fcsf | 0.166 | 0.166 |
| Blood flow rate in ml/min^b | | |
| Hipp_csf | 0.00002 | 0.00114 |
| FQcortex_csf | 0.00005 | 0.0566 |
| FQrb_csf | 0.00024 | 0.285 |

Fraction of volume and blood flows related to brain were taken from following reference (Delgado-Gonzalez et al., 2015; Zakaria and Badhan, 2018).

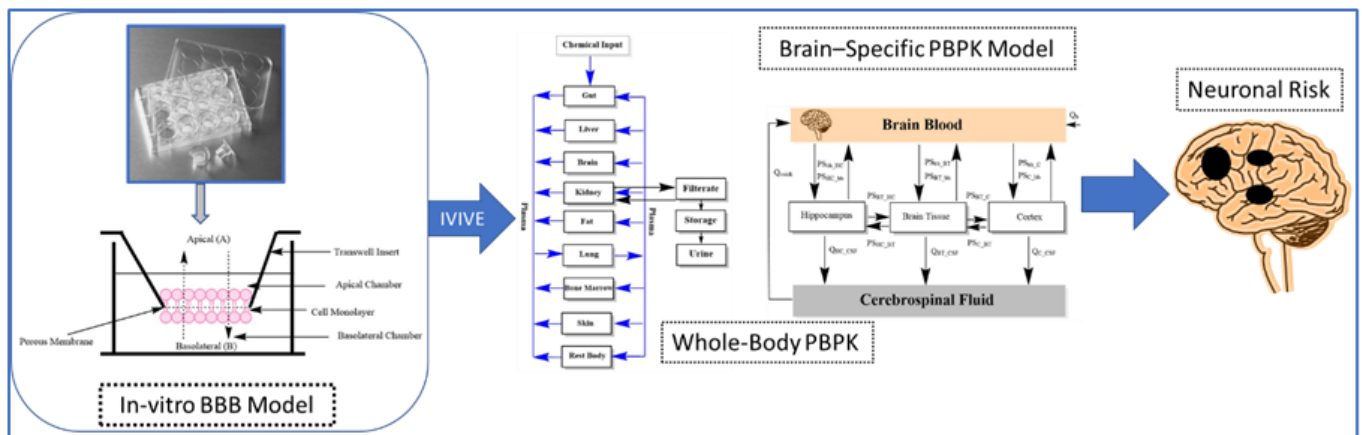


Fig 16: Integration of in-vitro transwell permeability data with brain specific PBK Model using mechanistic PBPK-IVIVE for evaluating neurotoxic risk assessment.

6.2.5 Exposure scenarios modelled

Rat brain PBK: Oral dose extracted from 2 papers were used as input for calculating brain hippocampal and cortex concentration in rats (Austin et al., 2003; Liu et al., 2010).

Human brain PBK: Low dose of 10 ng/kg was used as the input concentration to predict sub-compartment toxicokinetic.

6.3. Results

6.3.1 NAM testing results

The brain was modelled with permeability clearance from BB which was collected using in-vitro experiment. In-vitro experiment was done with human BBB cells (explained in above section). IVIVE (*in-vitro* to *in-vivo* extrapolation) approach was used to calculate the PS (Permeability Surface area product) for *in-vivo* from apparent permeability coefficient (Papp). Correction for endothelial surface area and brain weight was done accordingly as per eq. 4. In equation mentioned below, PS_{B_bb} refers to permeability for blood to brain, Papp_{A-B} refers to apical to basolateral permeability, brain weight is 1.8 gm in rat and 1550 gm in human, and brain surface area is 150 cm²*g*brain⁻¹ (rats), 157 cm²*g*brain⁻¹ (human). Similar equation can be applied for PS_{bb_B} (permeability from brain to blood) where Papp_{A-B} is replaced by Papp_{B-A}.

$$PS_{B_bb} = Papp_{A-B} * Brain\ weight * Surface\ area$$

6.3.2 PBK model results

Fig 17 shows the good agreement between experimental and simulated data at different doses of PFOS in rat. Dose dependent accumulation was observed in cortex concentration at oral exposure of 1 mg/Kg and 10 mg/kg for 14 days (Austin et al., 2003) and three doses of 1.75, 5 and 15 mg/L for 91 days (Liu et al., 2010). There was unusual data trend in hippocampus concentration which model was not able to capture. At 1 mg/kg, hippocampus concentration was almost half of cortex but at 10 mg/kg, this phenomenon reversed. It was observed that the clearance from hippocampus becomes quite low at 10 mg/kg which may be due to saturation of transporter. But there is no mechanism explained about this in literature. That’s why a correction factor was applied for hippocampus which becomes active only at higher dose. No data was available in literature for PFOA disposition in brain-sub compartment, so similar biochemical parameters as PFOS were considered. We observed that at similar doses, accumulation for PFOA in brain compartment is a little less compared to PFOS.

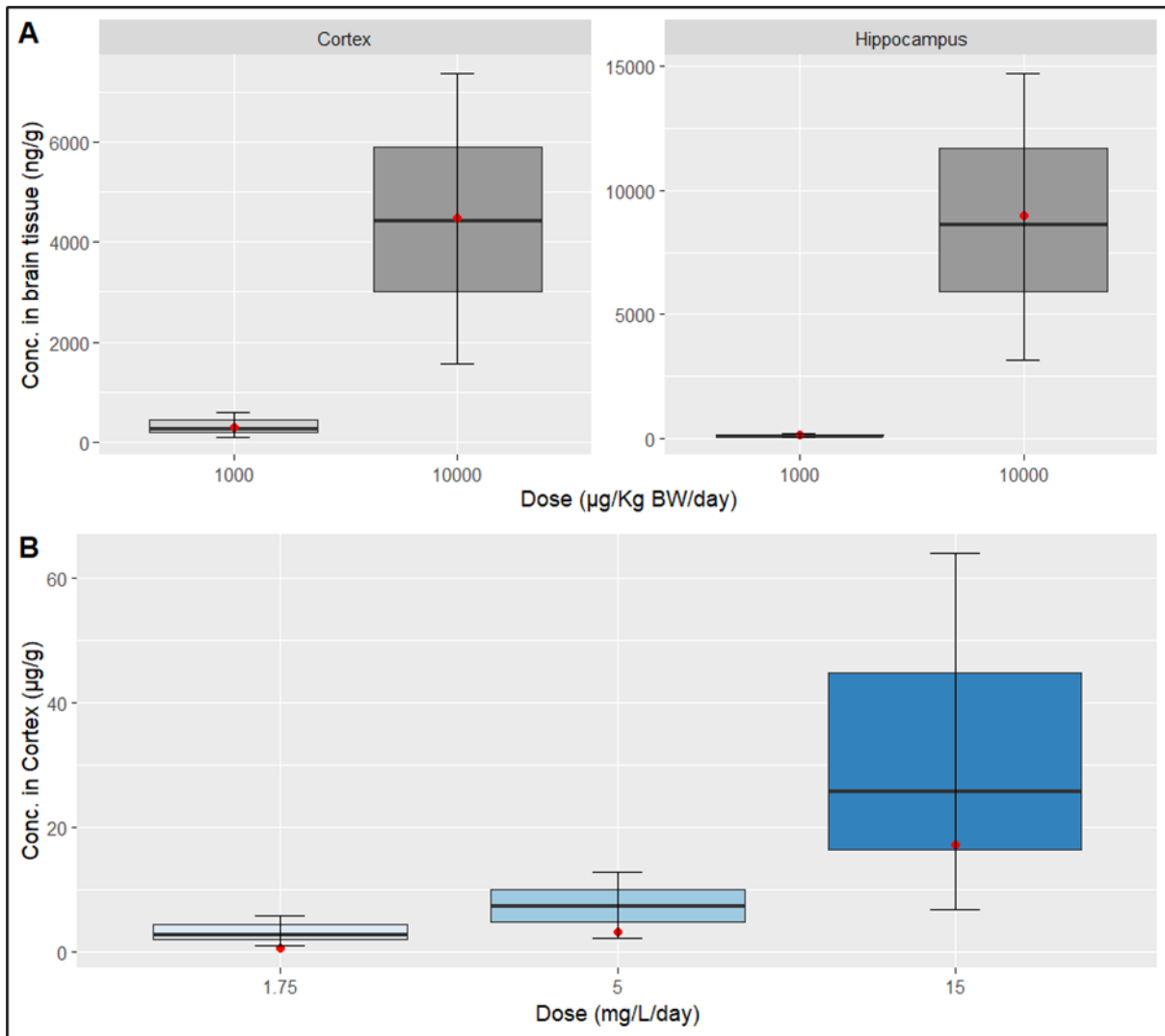


Fig 17: Observed and simulated hippocampus and cortex concentration in rat brain at different oral doses for PFOS (Austin et al., 2003; Liu et al., 2010). Upper whisker represents percentile 97.5 and lower whisker represents percentile 2.5. Red dot represents experimental data which is 294 ng/g and 4487 ng/g in cortex, and 115 ng/g and 8966 in hippocampus for plot A and 0.56, 3.25 and 17.21 ug/g in cortex for plot B respectively (Liu et al., 2010).

Fig 18 shows the simulated hippocampus and cortex concentration at PFOS dose (10 ng/Kg) for 10 years in adult human. It was found that concentration in plasma and brain reached steady state after 3-5 years of exposure. Cortex concentration was higher than hippocampus showing a slow and steady increase being affected by influx and efflux of the chemical. Similar dosing scenario was performed for PFOA adult human (not shown here) and simulated

concentration showed lower disposition in both sub-compartments compared to PFOS. The reason can be PFOS is having higher permeability through blood-brain-barrier compared to PFOA also observed in data obtained through permeability experiment performed using HCMEC/D3 cell line experiment and hence possess the risk for neuronal damage.

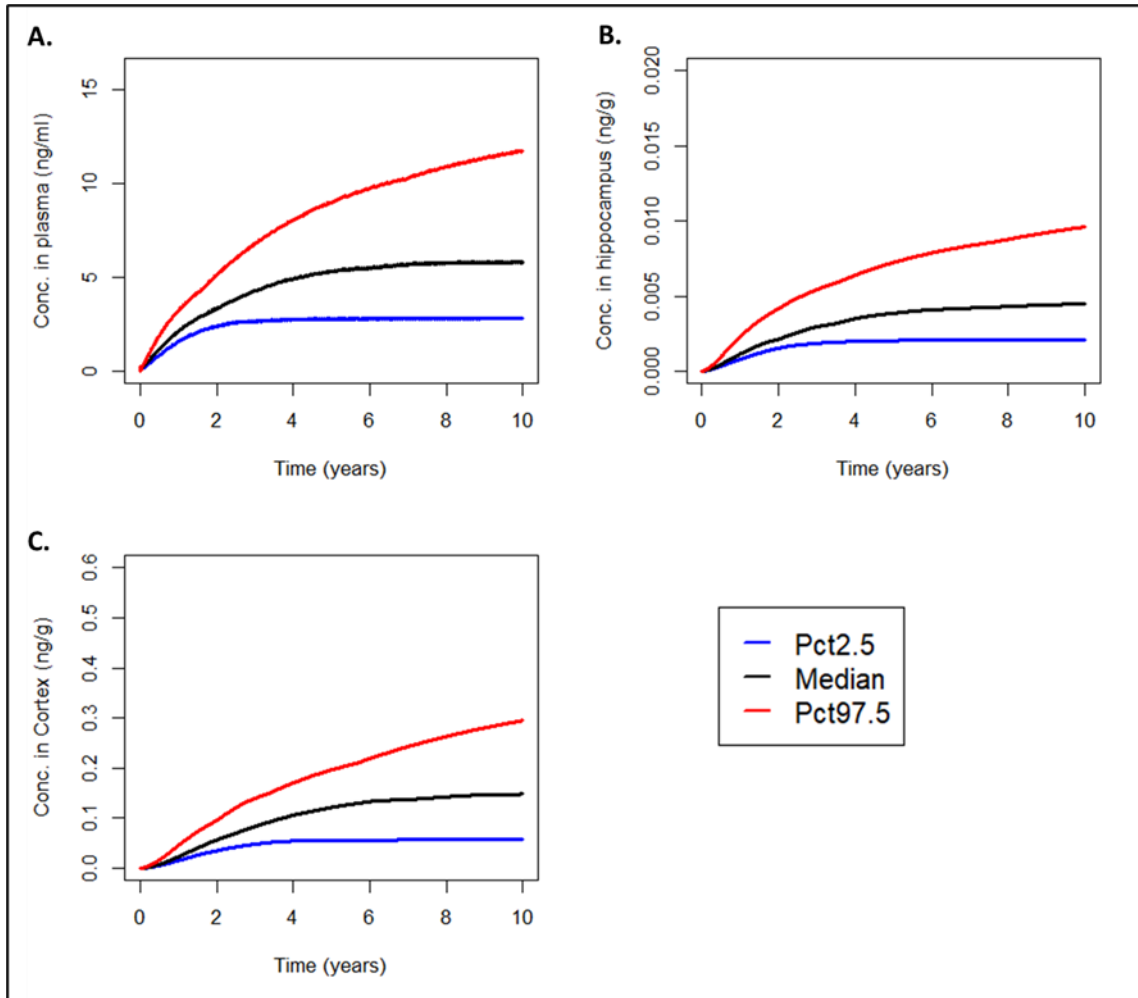


Fig 18: PFOS Concentration time plot in human plasma, hippocampus, and cortex after 10 ng/kg exposure for 10 years in adult human. Blue line represent percentile 2.5, black line represents median and red line represents percentile 97.5.

6.4. Discussion

6.4.1 Main learnings- what is new and what do we learn from this case study?

This case study has provided a framework about how *in-vitro* data from BBB cell lines can be successfully integrated into brain PBK reducing the need for animal studies. Additionally, we successfully applied the approach of doing IVIVE for brain PBK which can be extended further for other chemicals of interest. This model if combined with systems biology models can provide information about neurotoxic risk and also aid for quantifying key events in neurotoxicity related adverse outcome pathways (AOPs).

However, if more data on *in-vitro* is made available in future, this model could be improved further by incorporating separate fu for brain sub-compartment based on experimental data. The differences in lipid/water content can contribute to variation in fu levels and also the variation in these content in white and grey matter. Further *in-vitro* setup can be improved by adding albumin during the permeability experiment. In conclusion, this was the first

attempt to building a mechanistic brain-specific PBK model utilizing *in-vitro* data. We were able to successfully predict the brain concentration in rat hippocampus and cortex at different exposure level. It can be used in future for calculating oral equivalent dose based on *in-vitro* exposure to translate the result to human and animals. Integrating brain PBK with systems biology model can help in deciphering neuronal adverse pathways and predicting neurotoxicity in human beings.

7. Conclusion

In conclusion, the PARC project significantly advances the field of Next Generation Hazard and Risk Assessment (NGRA) by developing and applying innovative physiologically based kinetic models. These models integrate cutting-edge New Approach Methods (NAMs) such as *in silico* and *in vitro* techniques to enhance the understanding of compound-specific ADME characteristics. The detailed case studies presented provide valuable insights into the objectives, rationale, and outcomes of using these models, addressing crucial data and knowledge gaps.

This work not only underpins the importance of *In Vitro* to *In Vivo* Extrapolation (IVIVE) in setting human-relevant safety thresholds but also highlights ongoing challenges and future perspectives in refining the predictive accuracy and applicability of these models in risk assessment. Efforts are underway to present the case study at various conferences and internal PARC meetings, with the aim of demonstrating to regulatory agencies (EFSA, ECHA), the value of such model in translating neuronal risk and supporting its inclusion in future regulatory guidelines.

8. References

- Achour, B., Barber, J. and Rostami-Hodjegan, A. (2014). Expression of hepatic drug-metabolizing cytochrome p450 enzymes and their intercorrelations: A meta-analysis. *Drug Metab Dispos* 42, 1349-1356. doi:10.1124/dmd.114.058834
- Austin, M. E., Kasturi, B. S., Barber, M. et al. (2003). Neuroendocrine effects of perfluorooctane sulfonate in rats. *Environ Health Perspect* 111, 1485-1489. doi:10.1289/ehp.6128
- Balhara, A., Kumar, A. R. and Unadkat, J. D. (2022). Predicting human fetal drug exposure through maternal-fetal pbpk modeling and in vitro or ex vivo studies. *J Clin Pharmacol* 62 Suppl 1, S94-S114. doi:10.1002/jcph.2117
- Beaudouin, R., Micallef, S. and Brochot, C. (2010). A stochastic whole-body physiologically based pharmacokinetic model to assess the impact of inter-individual variability on tissue dosimetry over the human lifespan. *Regul Toxicol Pharmacol* 57, 103-116. doi:10.1016/j.yrtph.2010.01.005
- Bharal, B., Ruchitha, C., Kumar, P. et al. (2024). Neurotoxicity of per- and polyfluoroalkyl substances: Evidence and future directions. *Sci Total Environ* 955, 176941. doi:10.1016/j.scitotenv.2024.176941
- Brown, R. P., Delp, M. D., Lindstedt, S. L. et al. (1997). Physiological parameter values for physiologically based pharmacokinetic models. *Toxicol Ind Health* 13, 407-484. doi:10.1177/074823379701300401
- Buratti, F. M., Volpe, M. T., Meneguz, A. et al. (2003). Cyp-specific bioactivation of four organophosphorothioate pesticides by human liver microsomes. *Toxicol Appl Pharmacol* 186, 143-154. doi:10.1016/s0041-008x(02)00027-3
- Comenges, J. M. Z., Joossens, E., Benito, J. V. S. et al. (2017). Theoretical and mathematical foundation of the virtual cell based assay - a review. *Toxicol In Vitro* 45, 209-221. doi:10.1016/j.tiv.2016.07.013
- Deepika, D., Sharma, R. P., Schuhmacher, M. et al. (2021). Risk assessment of perfluorooctane sulfonate (pfos) using dynamic age dependent physiologically based pharmacokinetic model (pbpk) across human lifetime. *Environ Res* 199, 111287. doi:10.1016/j.envres.2021.111287
- Deepika, D., Kumar, S., Bravo, N. et al. (2022). Chlorpyrifos, permethrin and cyfluthrin effect on cell survival, permeability, and tight junction in an in-vitro model of the human blood-brain barrier (bbb). *Neurotoxicology* 93, 152-162. doi:10.1016/j.neuro.2022.09.010
- Delgado-Gonzalez, J. C., Mansilla-Legorburo, F., Florensa-Vila, J. et al. (2015). Quantitative measurements in the human hippocampus and related areas: Correspondence between ex-vivo mri and histological preparations. *PLoS One* 10, e0130314. doi:10.1371/journal.pone.0130314
- Di, L., Kerns, E. H., Fan, K. et al. (2003). High throughput artificial membrane permeability assay for blood-brain barrier. *Eur J Med Chem* 38, 223-232. doi:10.1016/s0223-5234(03)00012-6
- Fisher, C., Simeon, S., Jamei, M. et al. (2019). Vivd: Virtual in vitro distribution model for the mechanistic prediction of intracellular concentrations of chemicals in in vitro toxicity assays. *Toxicol In Vitro* 58, 42-50. doi:10.1016/j.tiv.2018.12.017
- Foxenberg, R. J., McGarrigle, B. P., Knaak, J. B. et al. (2007). Human hepatic cytochrome p450-specific metabolism of parathion and chlorpyrifos. *Drug Metab Dispos* 35, 189-193. doi:10.1124/dmd.106.012427
- Han, J., Fu, J., Sun, J. et al. (2021). Quantitative chemical proteomics reveals interspecies variations on binding schemes of I-fabp with perfluorooctanesulfonate. *Environ Sci Technol* 55, 9012-9023. doi:10.1021/acs.est.1c00509
- Janssen, A. W. F., Duivenvoorde, L. P. M., Beekmann, K. et al. (2024). Transport of perfluoroalkyl substances across human induced pluripotent stem cell-derived intestinal epithelial cells in comparison with primary human intestinal epithelial cells and caco-2 cells. *Arch Toxicol* 98, 3777-3795. doi:10.1007/s00204-024-03851-x
- Kansy, M., Senner, F. and Gubernator, K. (1998). Physicochemical high throughput screening: Parallel artificial membrane permeation assay in the description of passive absorption processes. *J Med Chem* 41, 1007-1010. doi:10.1021/jm970530e
- Kim, S. J., Choi, E. J., Choi, G. W. et al. (2019). Exploring sex differences in human health risk assessment for pfna and pfda using a pbpk model. *Arch Toxicol* 93, 311-330. doi:10.1007/s00204-018-2365-y
- Liu, X., Liu, W., Jin, Y. et al. (2010). Effects of subchronic perfluorooctane sulfonate exposure of rats on calcium-dependent signaling molecules in the brain tissue. *Arch Toxicol* 84, 471-479. doi:10.1007/s00204-010-0517-9
- Loccisano, A. E., Campbell, J. L., Jr., Andersen, M. E. et al. (2011). Evaluation and prediction of pharmacokinetics of pfoa and pfos in the monkey and human using a pbpk model. *Regul Toxicol Pharmacol* 59, 157-175. doi:10.1016/j.yrtph.2010.12.004
- Loccisano, A. E., Campbell, J. L., Jr., Butenhoff, J. L. et al. (2012). Comparison and evaluation of pharmacokinetics of pfoa and pfos in the adult rat using a physiologically based pharmacokinetic model. *Reprod Toxicol* 33, 452-467. doi:10.1016/j.reprotox.2011.04.006
- Mendez-Catala, D. M., Wang, Q. and Rietjens, I. (2021). Pbk model-based prediction of intestinal microbial and host metabolism of zearalenone and consequences for its estrogenicity. *Mol Nutr Food Res* 65, e2100443. doi:10.1002/mnfr.202100443

- Morris, M. D. (1991). Factorial sampling plans for preliminary computational experiments. *Technometrics* 33, doi:10.2307/1269043
- National Toxicology Program (2022a). Ntp technical report on the toxicity studies of perfluoroalkyl sulfonates (perfluorobutane sulfonic acid, perfluorohexane sulfonate potassium salt, and perfluorooctane sulfonic acid) administered by gavage to sprague dawley (hsd:Sprague dawley sd) rats (revised). . In (eds.), Research Triangle Park Available from: <https://www.ncbi.nlm.nih.gov/books/NBK551469/> doi:10.22427/NTP-TOX-96
- National Toxicology Program (2022b). Ntp technical report on the toxicity studies of perfluoroalkyl carboxylates (perfluorohexanoic acid, perfluorooctanoic acid, perfluorononanoic acid, and perfluorodecanoic acid) administered by gavage to sprague dawley (hsd:Sprague dawley sd) rats (revised): Toxicity report 97. . In (eds.), Available from: <https://www.ncbi.nlm.nih.gov/books/NBK551546/> doi:doi: 10.22427/NTP-TOX-97
- Neylon, J., Fuller, J. N., van der Poel, C. et al. (2022). Organophosphate insecticide toxicity in neural development, cognition, behaviour and degeneration: Insights from zebrafish. *J Dev Biol* 10, doi:10.3390/jdb10040049
- Nowak, N., Escher, S. E. and Schwarz, K. (submitted). A unified whole lung pbk model for inhalational uptake of gases and aerosols in men.
- Pastrakuljic, A., Tang, B. K., Roberts, E. A. et al. (1997). Distinction of cyp1a1 and cyp1a2 activity by selective inhibition using fluvoxamine and isosafrole. *Biochem Pharmacol* 53, 531-538. doi:10.1016/s0006-2952(96)00769-1
- Punt, A., Lousse, J., Beekmann, K. et al. (2022). Predictive performance of next generation human physiologically based kinetic (pbk) models based on in vitro and in silico input data. *ALTEX* 39, 221-234. doi:10.14573/altex.2108301
- Rosato, I., Bonato, T., Fletcher, T. et al. (2024). Estimation of per- and polyfluoroalkyl substances (pfas) half-lives in human studies: A systematic review and meta-analysis. *Environ Res* 242, 117743. doi:10.1016/j.envres.2023.117743
- Santori, N., Buratti, F. M., Dorne, J. C. M. et al. (2020). Phosmet bioactivation by isoform-specific cytochrome p450s in human hepatic and gut samples and metabolic interaction with chlorpyrifos. *Food Chem Toxicol* 143, 111514. doi:10.1016/j.fct.2020.111514
- Sibinovska, N., Zakelj, S., Roskar, R. et al. (2020). Suitability and functional characterization of two calu-3 cell models for prediction of drug permeability across the airway epithelial barrier. *Int J Pharm* 585, 119484. doi:10.1016/j.ijpharm.2020.119484
- Sun, D., Lennernas, H., Welage, L. S. et al. (2002). Comparison of human duodenum and caco-2 gene expression profiles for 12,000 gene sequences tags and correlation with permeability of 26 drugs. *Pharm Res* 19, 1400-1416. doi:10.1023/a:1020483911355
- Tebby, C., van der Voet, H., de Sousa, G. et al. (2020). A generic pbtk model implemented in the mcra platform: Predictive performance and uses in risk assessment of chemicals. *Food Chem Toxicol* 142, 111440. doi:10.1016/j.fct.2020.111440
- Tepper, S. J. and Johnstone, M. R. (2018). Breath-powered sumatriptan dry nasal powder: An intranasal medication delivery system for acute treatment of migraine. *Med Devices (Auckl)* 11, 147-156. doi:10.2147/MDER.S130900
- Testai, E., Bechaux, C., Buratti, F. M. et al. (2021). Modelling human variability in toxicokinetic and toxicodynamic processes using bayesian meta-analysis, physiologically-based modelling and in vitro systems. *EFSA Supporting Publications* 18, doi:10.2903/sp.efsa.2021.EN-6504
- Thakur, A., Parvez, M. M., Leeder, J. S. et al. (2021). Ontogeny of drug-metabolizing enzymes. In S. Nagar, Argikar, U.A., Tweedie, D. (eds) (eds.), *Enzyme kinetics in drug metabolism* New York, NY.: Humana. <https://link.springer.com/content/pdf/10.1007%2F978-1-0716-1554-6.pdf> doi:10.1007/978-1-0716-1554-6_18
- Timchalk, C., Nolan, R. J., Mendrala, A. L. et al. (2002). A physiologically based pharmacokinetic and pharmacodynamic (pbpk/pd) model for the organophosphate insecticide chlorpyrifos in rats and humans. *Toxicol Sci* 66, 34-53. doi:10.1093/toxsci/66.1.34
- Upreti, V. V. and Wahlstrom, J. L. (2016). Meta-analysis of hepatic cytochrome p450 ontogeny to underwrite the prediction of pediatric pharmacokinetics using physiologically based pharmacokinetic modeling. *J Clin Pharmacol* 56, 266-283. doi:10.1002/jcph.585
- Wang, Y. T., Mohammed, S. D., Farmer, A. D. et al. (2015). Regional gastrointestinal transit and ph studied in 215 healthy volunteers using the wireless motility capsule: Influence of age, gender, study country and testing protocol. *Aliment Pharmacol Ther* 42, 761-772. doi:10.1111/apt.13329
- Wen, Y., Qi, H., Ostergaard Mariager, C. et al. (2020). Sex differences in kidney function and metabolism assessed using hyperpolarized [1-(13c)]pyruvate interleaved spectroscopy and nonspecific imaging. *Tomography* 6, 5-13. doi:10.18383/j.tom.2020.00022
- Wetmore, B. A., Wambaugh, J. F., Allen, B. et al. (2015). Incorporating high-throughput exposure predictions with dosimetry-adjusted in vitro bioactivity to inform chemical toxicity testing. *Toxicol Sci* 148, 121-136. doi:10.1093/toxsci/kfv171
- Williams, A. J., Grulke, C. M., Edwards, J. et al. (2017). The comtox chemistry dashboard: A community data resource for environmental chemistry. *J Cheminform* 9, 61. doi:10.1186/s13321-017-0247-6
- Wilson, Z. E., Rostami-Hodjegan, A., Burn, J. L. et al. (2003). Inter-individual variability in levels of human microsomal protein and hepatocellularity per gram of liver. *Br J Clin Pharmacol* 56, 433-440. doi:10.1046/j.1365-2125.2003.01881.x

- Wohnsland, F. and Faller, B. (2001). High-throughput permeability ph profile and high-throughput alkane/water log p with artificial membranes. *J Med Chem* 44, 923-930. doi:10.1021/jm001020e
- Zakaria, Z. and Badhan, R. (2018). Development of a region-specific physiologically based pharmacokinetic brain model to assess hippocampus and frontal cortex pharmacokinetics. *Pharmaceutics* 10, doi:10.3390/pharmaceutics10010014